9.01 Interaction of Ionizing Radiation with Matter

B Nilsson, Stockholm University, Stockholm, Sweden
A Brahme, Karolinska Institutet, Stockholm, Sweden

Nomenclature

A	Atomic weight
b	Impact parameter
B_{nj}	Binding energy of an electron in shell n and subshell j
c	Velocity of light
$d\sigma/d\Omega$	Scattering cross section differential in solid angle Ω
e	Elementary unit of electric charge
E	Kinetic energy of charged particle
$F(q,Z)$	Atomic form factor, as function of momentum transfer, q, and atomic number, Z
g	Fraction of the kinetic energy lost by charged particles in radiative processes when the charged particles slow down to rest
$h\nu$	Photon energy at frequency ν
I	Mean excitation energy
k	Energy of photon expressed in electron mass units
L_Δ	Linear energy transfer or restricted (Δ) linear electronic stopping power
M	Rest mass of charged particle
m_e	Rest mass of electron (or positron)
N_A	Avogadro constant
p	Particle momentum
R	Radiant energy
r_e	Classical electron radius
$S(q,Z)$	Incoherent scattering factor, as function of momentum transfer, q, and atomic number, Z
$S(r,\theta)$	Angular distribution of bremsstrahlung
S_{el}/ρ	Mass collision stopping power
S_{nucl}/ρ	Mass nuclear stopping power
S_{rad}/ρ	Mass radiative stopping power
T/ρ	Mass scattering power
v	Particle velocity
X	Radiation length
$Y(E_o)$	Radiation yield for an electron with initial kinetic energy E_o
z	Charge of incident particle in units of the charge of the electron
Z	Atomic number
α	Fine structure constant
β	Ratio of particle velocity to the velocity of light
β/ρ	Absorption coefficient for β-radiation
δ	Density–effect correction
ε_o	Permittivity
$\Pi(x)$	Particle fluence at depth x
κ/ρ	Mass cross section for pair production
μ/ρ	Mass attenuation coefficient
μ_{en}/ρ	Mass energy absorption coefficient
μ_{tr}/ρ	Mass energy transfer coefficient
ρ	Density of the medium
σ	Cross section
σ/ρ	Mass cross section for scattering
$\sigma_{\gamma n}/\rho$	Mass cross section for photonuclear reaction
τ	The ratio of kinetic energy of a particle to its rest energy
τ/ρ	Mass cross section for photoelectric effect
ω	Fluorescence yield
$\Psi(x)$	Energy fluence at depth x

9.01.1 Introduction

There are several reviews of the interaction of ionizing radiation with matter, which are valuable for medical physics applications (e.g., Attix, 1986; Bethge et al., 2004; Evans, 1955; Khan, 2003; Nikjoo et al., 2012; Podgorsak, 2009; Roy and Reed, 1968), and the reader may refer to them and original publications for a more extensive description. The aim of this chapter is to give an overview and try to show how the different interaction probabilities will influence the transport of ionizing radiation through matter. This knowledge is important in different aspects of medical applications of radiation. It has an impact in designing an optimal treatment gantry, in the choice of radiation quality and of course when determining the absorbed dose distribution in the body. It is also important in diagnostic radiology when optimizing the image quality. Knowledge of interaction of radiation with matter is also fundamental for understanding the biological effect of radiation and its variation with ionization density. The focus will not be on the basic physics and deriving the different cross sections but on the impact of these cross sections on imaging and therapy in medical physics applications. This chapter will then not include detailed data on cross sections or tables found in the published literature (e.g., Higgins et al., 1991; ICRU, 1984a,b, 1993) or on the Internet (e.g., Berger et al., 2005a,b; http://nist.gov./pml/data/). The notations proposed by ICRU (ICRU, 2011) will be used when relevant.

Ionizing radiation is normally divided into charged particles (previously called directly ionizing radiation) such as leptons, α-particles, protons and other light ions, and uncharged particles (previously called indirectly ionizing radiation) such as photons (x-rays or γ-rays) and neutrons. This chapter will concentrate on radiation qualities used in radiotherapy, and the main part will be dedicated to electrons and photons with

energies up to around 50 MeV and light ions with energies up to 900 MeV per nucleon. The presentation is divided into two main sections, charged particles and photons.

9.01.2 Charged Particles

9.01.2.1 Introduction to Charged Particle Interaction

When charged particles pass through matter, their Coulomb electric field will interact with the atomic electrons and the atomic nuclei in the matter. Normally, only a small part of the kinetic energy is lost in each collision, and the particles will undergo several interactions before they have transferred all their kinetic energy to matter. The interactions will give rise to excitations and ionizations of the atoms and emission of electromagnetic radiation, often called bremsstrahlung. Depending on the type of charged particle, different interaction processes are more or less important, and often, the description of the interactions of charged particles is divided into light charged particles (electrons and positrons) and heavy charged particles (ions). The ions are sometimes further divided into light ions with $Z \leq 10$ and heavy ions with $Z \geq 10$. The choice of Z is somewhat arbitrary. Figure 1 describes in a simplified way the transport of charged particles in matter for ions and electrons. The mechanisms by which charged particles lose energy or are scattered can be divided into four principal types of interactions:

1. *Inelastic collision with atomic electrons*. This is the dominant mechanism by which heavy charged particles and light charged particles with low to medium energy will lose their energy. As a result of such a collision, there will be excitations and ionizations. Often, the energy transferred to the emitted electron may be high enough to make it possible for the electron to ionize new atoms. If the energy is low, only a few atoms will be ionized and there will be a cluster of often three to four ionizations close to each other. If the energy is higher, this secondary electron is called a δ-electron.
2. *Inelastic collision with a nucleus*. When a charged particle passes near a nucleus, it will be deflected. In some of the deflections, the charged particle will lose energy and this energy is emitted as electromagnetic radiation called bremsstrahlung. This interaction process is, in the energy region used in medical physics, only of interest for electrons and positrons.
3. *Elastic scattering with a nucleus*. When the particle is deflected without exciting the nucleus or emitting radiation, there will be elastic scattering. Not only light charged particles but also heavy charged particles, in particular low-energy particles, have a high probability for experiencing elastic scattering.
4. *Elastic collision with atomic electrons*. An incident electron may be elastically deflected in the field of the atomic electrons. These processes are of interest only for very-low-energy electrons and will not be discussed in this chapter.

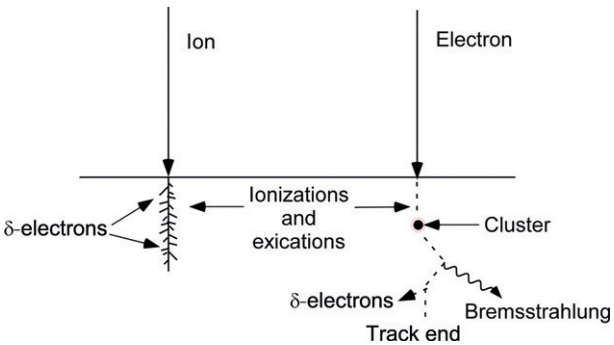

Figure 1 Schematic diagram of the transport of an ion and an electron through matter.

As indicated in Figure 1, the tracks of the charged particles will differ from both macroscopic and microscopic points of view. The heavy charged particle will excite and ionize atoms along its path. As the particle is heavy compared to the electrons, it will only transfer a very small amount of its energy in each collision and will only be deflected in elastic scattering with the nucleus. The track is then rather straight and different particles will have a similar range. The produced δ-particles will also have low energies. However, a light particle can lose a large part of its energy in one collision and can be deflected at large angles. They can also produce high-energy δ-particles and bremsstrahlung. This means that different electron tracks will differ significantly leading to a large energy and range straggling as will be discussed in the following sections.

9.01.2.2 Inelastic Collisions of Heavy Charged Particles with Atomic Electrons and Nuclei

9.01.2.2.1 Inelastic collisions with atomic electrons

Figure 2 shows a sketch of a collision between a heavy charged particle with the charge ze and the mass M and an atomic electron with the charge e and mass m_e. The impact parameter b is the closest distance between the particle and the electron without any deflection of the particle. If b is similar to the radius of the atom, the Coulomb force interaction will transfer a large energy to the electron and then the interaction is called a *hard* collision. If on the other hand, b is much larger than the atomic radius, a small energy is transferred, and the interaction is called a *soft* collision. The discussions in this section refer mainly to the situation for soft collisions, which are the most common ones. Bohr (1913a,b) derived, using classical physics, an expression for the energy loss for heavy charged particles, where only electromagnetic forces were included. Bohr assumed that the velocity v of the charged particle is much larger than that of the orbital electrons. He also assumed that the electron can be regarded free and that the energy loss is small, which means that the heavy particle will not be deflected and the velocity will be constant before and after the interaction. The force, F, between the particles is given by

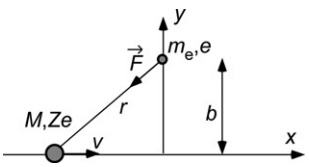

Figure 2 A simplified illustration of a collision between a heavy charged particle and an electron.

$$F = \frac{1}{4\pi\epsilon_0}\frac{ze^2}{r^2}\hat{r} \quad [1]$$

where ze is the charge of the incoming particle, e is the charge of the electron, r is the distance between the particle and the electron, and ϵ_0 is the dielectric constant in vacuum. With the aforementioned assumptions and integrating the energy transfer over all distances r, the relation between energy transfer ΔE and impact parameter b will become

$$\Delta E = \frac{4z^2e^4}{2(4\pi\epsilon_0)^2b^2v^2m_e} \quad [2]$$

where v is the velocity of the particle and m_e is the electron rest mass. The energy transfer ΔE is inversely proportional to the velocity of the particle in square; proportional to the particle charge in square, ze; and independent of the particle mass.

All energy transfers are not possible however. There is a maximal energy transfer based on energy and momentum relations. In the maximum energy transfer, the electron will be emitted in the forward direction. It is easy to show that the maximum energy transfer in such a collision is

$$\Delta E_{max} = \frac{4m_eE}{M} \quad [3]$$

where E is the kinetic energy of the incident particle. For heavy charged particles with masses more than 1000 times than the mass of the electron, this means that the energy transfers are very small. For example, will an 8 MeV α-particle transfer less than 0.4% of its energy. The relations will result in a maximum velocity of the electron twice of the velocity v of the incoming particle, that is, $2v$. This implies that the maximum energy transfer and thus the minimum impact parameter b are given by

$$\Delta E_{max} = 2m_ev^2 \Rightarrow b_{min} = \frac{ze^2}{4\pi\epsilon_0v^2m_e} \quad [4]$$

For a free electron, all energy transfers down to zero are possible. For orbital electrons, this is not possible. Bohr in his classical derivation compared the velocity of the particle and the orbital period ω and postulated that the minimum energy transfer corresponds to the situation when the velocity of the incoming particle equals the velocity of the orbital electrons. The minimal energy transfer and thus the maximal impact parameter are then given by

$$b_{max} = \frac{v}{\omega} \Rightarrow \Delta E_{min} = \frac{2z^2e^4\omega^2}{(4\pi\epsilon_0)^2v^4m_e} \quad [5]$$

The probability for an energy transfer between ΔE and $\Delta E + \mathrm{d}\,\Delta E$ is equal to the probability of an impact parameter between b and $b + \mathrm{d}b$. This is given by

$$\mathrm{d}\sigma = \frac{2\pi r_e^2m_ec^2z^2}{\beta^2}\frac{\mathrm{d}\,\Delta E}{\Delta E^2} \quad [6]$$

where c is the velocity of light in vacuum, $\beta = v/c$, and r_e is the classical electron radius defined as

$$r_e = \frac{e^2}{4\pi\epsilon_0m_ec^2} = 2.818 \cdot 10^{-15}\,\mathrm{m} \quad [7]$$

From this equation, the conclusion can be made that the probability to obtain a certain energy transfer ΔE is inverse to the energy transfer squared. This means that small energy transfers are more probable. Assuming that all impinging particles are uniformly distributed with the same probability for all values of b, the number of collisions $\mathrm{d}n$ with an energy transfer between ΔE and $\Delta E + \mathrm{d}\,\Delta E$ will be equal to the number of electrons per unit area times the collision cross section $\mathrm{d}\sigma$. The energy loss per distance $\mathrm{d}x$ in a material with (N_AZ/A) number of electrons per unit mass is then given by

$$\mathrm{d}\,\Delta E/\rho = (N_A/A)Z\mathrm{d}x\mathrm{d}\,\Delta E \quad [8]$$

Integrating over all energy losses from E_{min} to E_{max} gives the Bohr relation for the collision stopping power:

$$S_{el}/\rho = \frac{\mathrm{d}E_{el}}{\rho\mathrm{d}x} = 4\pi\frac{ZN_A}{A\beta^2}r_e^2z^2m_ec^2\ln\left(\frac{4\pi\epsilon_0m_ev^3}{ze^2\omega}\right) \quad [9]$$

This equation is however not correct and gives values that differed from experiments. At higher energies, the Bohr collision stopping power follows the trend of experimental data but with a factor of two too low, and in particular, at low energies, it completely fails to give correct values. To improve the expression, corrections must be added for (a) relativistic effects, (b) mean excitation energy, (c) impact of atomic electron shells, (d) effective charge, and (e) density effects.

The *relativistic corrections* are needed as at high velocities, the Lorentz contraction of the electric field increases the force at large distances. Thus, a velocity factor has to be included in the equation.

The *mean excitation energy*, I, accounts for all possible atomic ionizations and excitations and corresponds to the minimum energy that can be transferred on average to the absorbing atom in a Coulomb interaction between a charged particle and an orbital electron. I corresponds to the situation discussed earlier for the minimum energy transfer in a collision between the charged particle and the orbital electron. In principle, I can be calculated from the equation

$$Z\ln I = \sum f_{n0}\ln(E_n - E_0) \quad [10]$$

where 0 and n are the ground and the final energy levels of a target atom Z. f_{n0} is called the oscillator frequency and gives the probability for transitions between levels n and 0. It is however difficult to calculate I values theoretically, and they are often determined experimentally. During the years, values that differ with up to 10% have been published. This will imply uncertainties in the numerical values of the stopping power. At high particle energies, this uncertainty is not so important. At 100 MeV proton energy, an uncertainty in the I value of 1% will result in an uncertainty in the stopping power of less than 0.2%, but at low energies and high atomic numbers, the uncertainty in the I value will be fully expressed. The I value increases with atomic number and is around $I = 10Z$ except for low atomic numbers.

The concept *effective charge* is included for low particle energies where the particle can pick up electrons and thus the particle charge will be decreased. An α-particle will decrease its effective charge of 2 to 1.87 at 1 MeV and to 1.63 at 0.5 MeV. It is this effective charge that shall be included in the expressions for stopping power.

Bethe (1930) extended the Bohr expression to include also hard collisions based on the Born approximation and included relativistic effects. His expression is given in eqn [11]:

$$S_{el}/\rho = \frac{4\pi N_A r_e^2 m_e c^2 z^2 Z}{A\beta^2}\left\{\ln\frac{2m_e c^2}{I} + \ln\frac{\beta^2}{1-\beta^2} - \beta^2\right\} \quad [11]$$

This expression gives reasonable values as compared with experiments for energies down to about 0.5 MeV but fails at lower energies.

One reason for the failure is the impact of the *atomic electron shells*. When the velocity of the charged particles is comparable to the velocity of the orbital electron, the energy transfer decreases as also considered by Bohr. This effect is included in the stopping power by adding a shell correction factor C/Z.

Another reason is that Bethe considered each atom separately and independently. However, this is not correct. The electric field of the incoming particle induces a distortion or polarization of the atomic electrons. A number of dipoles are produced. This polarization decreases the effective charge of the incoming particle and thus reduces the stopping power. This effect is dependent on the density of the medium and is also called *density effect*. The effect becomes more important with increasing particle energy and partly compensates the increase in stopping power due to the Lorentz contraction. This effect is more important for electrons and positrons and of minor importance for heavy charged particles.

Fano (1946, 1953) included these correction factors in the Bethe stopping power equation and obtained the expression

$$S_{el}/\rho = \frac{4\pi N_A r_e^2 m_e c^2 z^2 Z}{A\beta^2}\left\{\ln\frac{2m_e c^2}{I} + \ln\frac{\beta^2}{1-\beta^2} - \beta^2 - \frac{C}{Z} - \delta\right\} \quad [12]$$

In Figure 3, the mass collision stopping power for protons expressed in MeV $m^2\,kg^{-1}$ obtained from the NIST program PSTAR is plotted for carbon, aluminum, copper, and lead. The data illustrate the effect due to the binding energies of the shells, giving lower stopping power at low proton energies. At high energies, the decrease with velocity as $1/v^2$ is observed. The collision stopping power is also lower for higher atomic numbers as the effect of the binding energies will be more important. The relativistic effects at very high energies above 2000 MeV are also indicated.

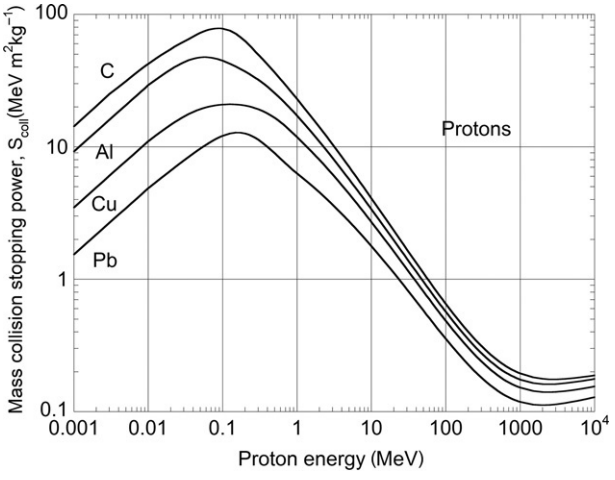

Figure 3 Mass collision stopping powers for carbon, aluminum, copper, and lead. Data from Berger et al. (2005b).

9.01.2.2.2 Nuclear reactions

There are also interactions with nuclei. These interaction processes are normally not important, but can at low proton energies be some percent of the total stopping power. For protons, the contribution from nuclear interactions is small, but for α-particles, there is a small but significant contribution at low energies (Figure 4). This uncertainty is important in radiotherapy with light-ion beams. Hultqvist et al. (2012) had investigated the uncertainties obtained in the dose distributions calculated with Monte Carlo programs due to differences in the cross sections. This implies the need for experimental verification, and then, the use of an online PET camera would be of interest as proposed by Lazzeroni and Brahme (2011), who suggested the use of carbon-11 ions to increase sensitivity. The interaction by ions with nuclei and its impact on radiotherapy with light ions are further discussed in Chapter 9.03, where the transport and interaction of light ions are discussed in detail.

9.01.2.2.3 Scaling rules

Tables for proton stopping power and ranges are often easy to find, for example, at NIST (http://nist.gov./pml/data/). With a good approximation, the mass collision stopping power for other heavy charged particles can be obtained from the proton stopping power through the relation

$$\frac{\left(\frac{dE}{\rho dx}\right)^A}{\left(\frac{dE}{\rho dx}\right)^B} = \left(\frac{z_A}{z_B}\right)^2 \quad [13]$$

A more accurate universal energy range relation was developed by Kempe and Brahme (2008).

9.01.2.3 Inelastic Collisions of Electrons and Positrons with Atomic Electrons

The equations for electrons and positrons differ from the relations obtained for heavy charged particles, and further correction factors have to be added as listed:

1. Electrons and positrons can lose a large part of their energy in one collision. This will imply that the electrons can be scattered in large angles and that hard collisions are more important.
2. Relativistic effects are more important.
3. Maximal energy transfer is $E/2$ for electrons and E for positrons, where E is the kinetic energy. An electron can transfer all of its kinetic energy to another electron in a collision. After the collision, there will be two electrons with different energies, and by convention, the electron with the highest energy is considered to be the primary one, and thus, the maximal energy transfer will be $E/2$. For positrons, it is possible to differentiate between the particles after the collision, and thus, the maximum energy transfer is E.
4. Density effect is more important than for heavy charged particles as discussed earlier. Figure 5 shows the density effect for electrons for water, copper, and lead. At low electron energies, the effect is small but increases with increasing electron energy and is significant at energies often met in radiotherapy. This is one of the main reasons

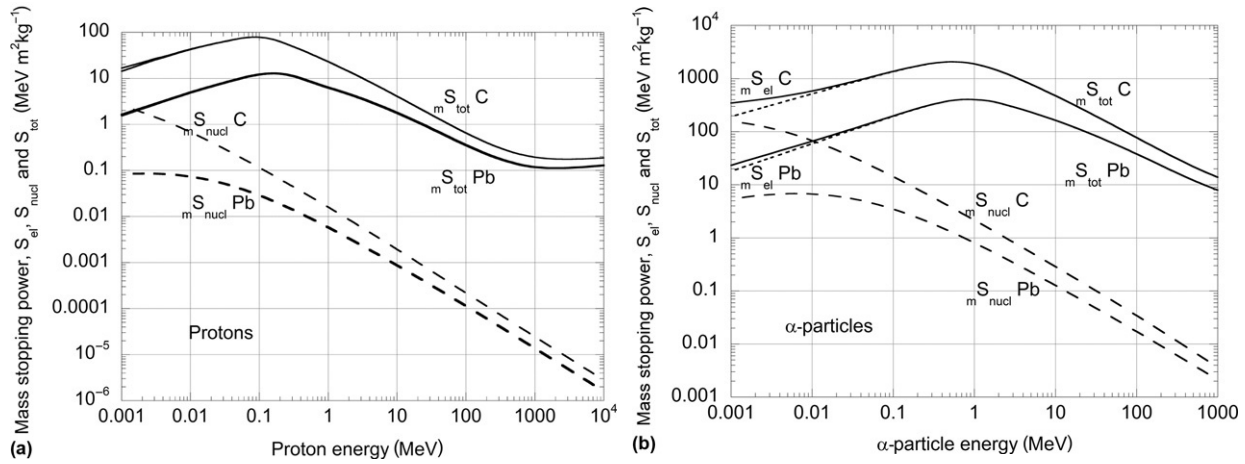

Figure 4 Mass stopping powers, (S_{el}/ρ), (S_{nucl}/ρ), and (S_{tot}/ρ), for protons and α-particles for carbon and lead. Data from Berger et al. (2005b).

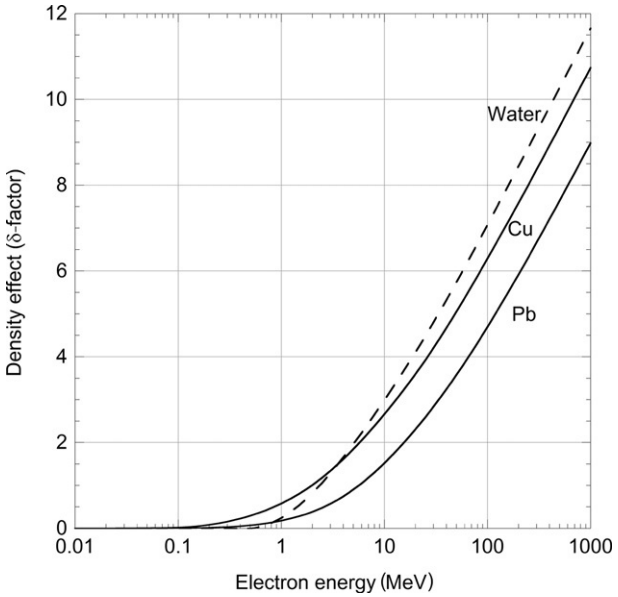

Figure 5 Density effect parameter δ for electrons in water, copper, and lead. Data from Berger et al. (2005b).

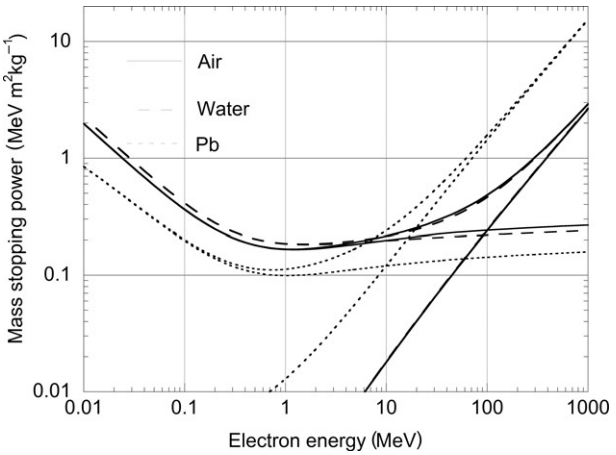

Figure 6 Mass stopping power (S_{el}/ρ), (S_{rad}/ρ), and (S_{tot}/ρ) for electrons in air, water, and lead. Data from NIST (2005).

that the stopping power ratio water/air varies with energy, indicating that from that point of view, the widely used air ionization chamber is less suitable. Another comment to be made is that many chambers have walls made of carbon as this is an air-equivalent element. Published stopping power tables have often tables for two forms of graphite, amorphous graphite with the density of 2200 kg m^{-3} and graphite with the bulk density of 1700 kg m^{-3} leading to different density factors. This difference in density will change the collision stopping power with around 0.5%.

In ICRU Report 37 (ICRU, 1984b) the mass collision stopping power for electrons and positrons is expressed as

$$S_{el}/\rho = r_e^2 \frac{Z}{A} N_A \frac{m_e c^2}{\beta^2}\left[\ln\left(\frac{E}{I}\right)^2 + \ln(1+\tau/2) + F^{\pm}(\tau) - \delta\right] \quad [14]$$

$F^{\pm}(\tau)$ are functions to be applied for the positron and electron, respectively, and are given by

$$F^{-}(\tau) = \left(1-\beta^2\right)\left[1+\tau^2/8-(2\tau+1)\ln 2\right] \quad [15]$$

and

$$F^{+}(\tau) = 2\ln 2 - \left(\beta^2/12\right)\left[23+14/(\tau+2)+10/(\tau+2)^2 + 4/(\tau+2)^3\right] \quad [16]$$

τ is the kinetic energy of the electron or positron expressed in electron rest masses, $\tau = E/(m_e c^2)$. Figure 6 shows mass collision stopping power for air, water, and lead, together with radiative and total stopping power. At low energies, there is an $1/v^2$ dependence on energy implying a decreasing stopping power with energy. The relativistic effects are the reason for the increase in stopping power in the energy region 1–10 MeV. For low energies, the mass collision stopping power for water is around 10% higher than the mass collision stopping power for air, but due to the density effect, air will have a higher stopping power for energies above 10 MeV. For electron energies below 0.01 MeV, the binding effects of the orbital electrons will be

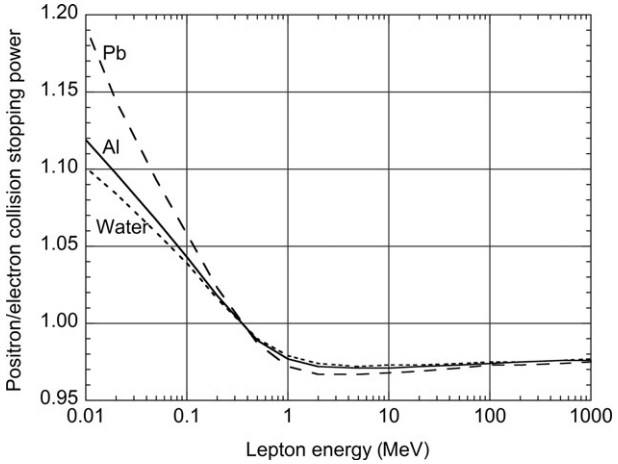

Figure 7 Ratio of collision stopping power for positrons to electrons.

important also for electrons, and the collision stopping power will decrease with decreasing energy. In medical applications, these energies are of less interest and also the uncertainties are large at these energies and tables have normally 0.01 MeV as a starting energy, why this decrease is not included in the figure.

Positrons have a slightly different collision stopping power as obtained from eqn [14]. At high energies, the difference is small, with the collision stopping power for electrons being slightly higher, but below approximately 1 MeV, the positron collision stopping power will become larger than the electron stopping power. The ratio between the two collision stopping powers increases with decreasing energy as shown in Figure 7.

9.01.2.3.1 Cerenkov radiation

A special type of collision loss is Cerenkov radiation, discovered by Cerenkov (Cerenkov, 1934). If a charged particle with a velocity larger than the velocity of light in a medium, that is, if $v \geq c/n$ (n = refractive index), passes through a transparent dielectric medium, electromagnetic radiation will be emitted (see Figure 8). The emission is due to polarized atoms in the medium and their orbital electrons may emit radiation coherently if $v \geq c/n$. The radiation, with a frequency in the UV and blue part of the spectrum, is emitted in a cone (Figure 8). The blue light seen above the open reactor tanks is a result of this effect. The threshold is low for electrons, in PMMA 0.175 MeV, while for protons, the threshold is 320 MeV. The energy loss is small, around 1 keV cm^{-1} in water for electrons, and has little impact on the total stopping power. From Figure 8, it can be shown that there is a relation between the light emission angle θ and the particle energy ($\cos\theta = 1/(\beta n)$). In this way, Cerenkov detectors have been used to determine particle energies.

The Cerenkov radiation can be a problem when detecting ionizing radiation using detectors based on measuring light as film or scintillation detectors, where unwanted Cerenkov radiation can disturb the measurements.

9.01.2.3.2 Restricted mass collision stopping power

In dosimetry, one is often interested in determining the energy transferred and the absorbed dose to a small volume, for example, an ionization chamber. If the contribution from secondary electrons (δ-particles) can be assumed to be

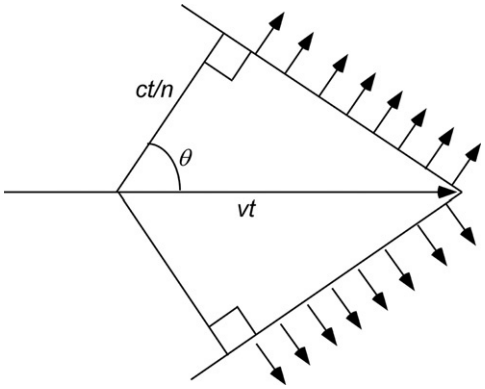

Figure 8 Cerenkov radiation is obtained when the velocity of the charged particle, v, is larger than the velocity of light in the material, c/n, where n is the refractive index of the material.

absorbed directly, the absorbed dose can be obtained by multiplying the particle fluence with the mass collision stopping power. This may be an acceptable approximation for heavy charged particles as then the δ-particles have a very low energy and a small range. However, this does not hold for electrons and positrons, where the secondary electrons can have energies in the same range as the primary electrons. To take this into consideration, the concept of restricted mass stopping power, $(S_{el}/\rho)_\Delta$, which includes only energy transfers below a certain energy limit Δ, is used. A common way to estimate the Δ-value is to compare the range of electrons with energy Δ and the size of the volume of interest. Ionization chambers are of particular interest in medical physics applications, and for typical ionization chambers used in radiotherapy, a Δ-value of 10 keV is often used.

A concept very similar to the restricted mass collision stopping power is linear energy transfer (LET) or the restricted linear electronic stopping power, which often is used to specify radiation quality. It is defined as the quotient of dE_Δ by dl, where dE_Δ is the mean energy lost by charged particles due to electronic interactions in traversing a distance dl, minus the mean sum of kinetic energies in excess of Δ of all the electrons released by the charged particles; thus,

$$L_\Delta = \frac{dE_\Delta}{dl} \quad \mathrm{J\,m^{-1}} \text{ or } \mathrm{keV\,\mu}m^{-1} \qquad [17]$$

The SI unit for LET is J m^{-1}, but in biological applications, still the unit keV μm^{-1} is often used. Δ is often expressed in the unit eV, and then, L_{100} means the LET with a cutoff energy of 100 eV. Figure 9 shows the restricted stopping power in carbon for cutoff energies 10 and 100 keV.

9.01.2.4 Bremsstrahlung

When a charged particle experiences an acceleration, it will, according to classical theory, emit electromagnetic radiation. This means that when a charged particle is deflected from its path or has its velocity changed due to an inelastic collision with a nucleus, it will start to irradiate. This emitted electromagnetic radiation is often called bremsstrahlung radiation. In classical theory, the power emitted in such a collision is given by

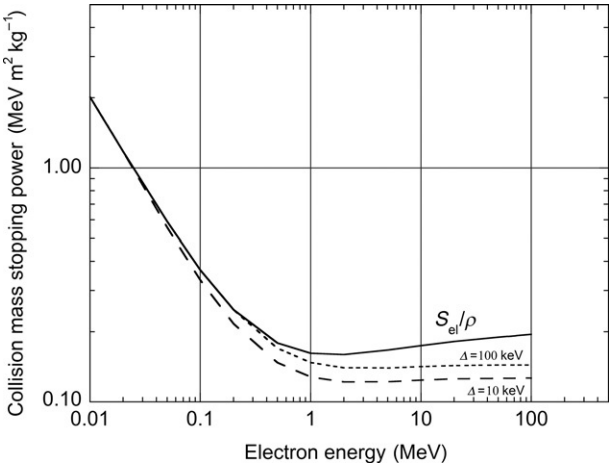

Figure 9 Restricted collision stopping power in carbon for the cutoff energies $\Delta = 10$ and 100 keV.

$$P = \frac{dE}{dt} = \frac{1}{6\pi\epsilon_0}\frac{e^2a^2}{c^3} \qquad [18]$$

where e is the charge of the particle and a is the acceleration. This holds for a stationary target. In a linear accelerator where the electrons are accelerated along a waveguide, the emitted power is given by

$$P = \frac{dE}{dt} = \frac{1}{6\pi\epsilon_0}\frac{e^2}{m^2c^3}\left(\frac{dE}{dx}\right)^2 \qquad [19]$$

where the power is also proportional to the change in the energy of the particle per unit distance in square. The acceleration may be evaluated in terms of both a Coulomb and a Newton force and is obtained from the relation

$$F = ma = \frac{zeZe}{4\pi\epsilon_0 r^2} \Rightarrow a = \frac{zeZe}{4m\pi\epsilon_0 r^2} \qquad [20]$$

where Ze is the charge of the nucleus and m is the mass of the incident particle. Equation [20] shows that the acceleration a is proportional to the charge of the particle and the absorbing nucleus and inversely proportional to the mass of the incident particle and the square of the distance r between the particle and the nucleus. This implies that bremsstrahlung can be neglected for protons compared to electrons as $m_p/m_e = 1836$, and thus, the bremsstrahlung emission is around 4×10^6 less for protons as compared to electrons.

9.01.2.4.1 Angular distribution

The angular distribution of the bremsstrahlung is given by

$$S(r,\theta) = \frac{1}{16\pi^2\epsilon_0}\frac{e^2a^2}{c^3r^2}\frac{\sin^2\theta}{(1-\beta\cos\theta)^5} \qquad [21]$$

From eqn [21], one can conclude that for low energies and thus low values of β, $S(r, \theta)$ is proportional to $\sin^2\theta$ with a maximum intensity at 90°. With increasing energy, the radiation becomes more forward-directed and the angle for maximal energy fluence is given by

$$\theta_{max} = \arccos\left\{\frac{1}{3\beta}\left(\sqrt{1+15\beta^2}-1\right)\right\} \qquad [22]$$

Equation [22] has the limits $\theta_{max} = 90°$ and 0° when the energy goes to 0 and ∞, respectively. The variation in angular distribution with electron energy is reflected in the practical production of bremsstrahlung in medical physics. In diagnostic radiology, where accelerating energies often are around 100 keV or lower, the useful beam is at an angle of 90° of the impinging electrons. Linear accelerators, with electron energies even above 20 MeV, have transmission targets, and the useful beam is in the same direction as the impinging electrons.

With high electron energies over 10 MeV, θ_{max} will be small and less than around 1°. This indicates that with increasing electron energy, the possibility to obtain a broad uniform beam is difficult and it may be problematic to flatten the bremsstrahlung beam with a traditional flattening filter. However, the equations hold for thin targets. In real targets, the angular distribution is broadened as most of the electrons will be scattered before they emit radiation. As the scattering power is proportional to Z^2, large-atomic-number targets will scatter electrons more and broaden the emitted bremsstrahlung.

A simple analytic approximation for the angular distribution of the energy fluence from a target is

$$\Psi(\theta) = \frac{\Psi(0)}{1+\left(\frac{E_0\theta}{a}\right)^b} \qquad [23]$$

where a is the value of $E_0\theta$ when $\Psi(\theta)/\Psi(0)$ is 0.5 and b is an energy-related constant (Brahme and Svensson, 1979).

In stationary treatment beams, a broad uniform beam is often requested and then large-atomic-number targets may be of interest. For accelerators with a scanning beam, a narrow beam with a high photon fluence in the forward direction is of interest. For these accelerators, a low atomic target may be used even if the total emitted radiation power is low (Svensson and Brahme, 1996).

9.01.2.4.2 Energy distribution

The energy distribution of the emitted bremsstrahlung radiation can be written as (Heitler, 1954)

$$\frac{d\sigma_{rad}}{dh\nu} = \alpha r_e^2 B(Z) Z^2 \frac{E + m_e c^2}{E}\frac{1}{h_\nu} \qquad [24]$$

The function $B(Z)$ is a slowly varying function with energy and often assumed to be constant up to the maximal photon energy, which is equal to E. This holds for a thin target. In a thick target, the electrons will lose energy when passing through a target. Adding the contribution from all depths in the target will give an approximative triangular shape when disregarding the self attenuation of the produced bremsstrahlung in the target and assuming that the production of bremsstrahlung is independent of energy in this energy range (**Figure 10(a)**). The distribution is given by

$$\Psi_{h\nu} = CZ(h\nu_{max} - h\nu) \qquad [25]$$

where C is a constant depending on the atomic number. This relation is sometimes called Kramer's law. The total energy fluence is obtained by integrating over all energies:

$$\Psi = CZ\int_0^{h\nu_{max}} (h\nu_{max} - h\nu)\, d(h\nu) = \frac{1}{2}CZ(h\nu_{max})^2 = \frac{1}{2}CZ(Ue)^2 \qquad [26]$$

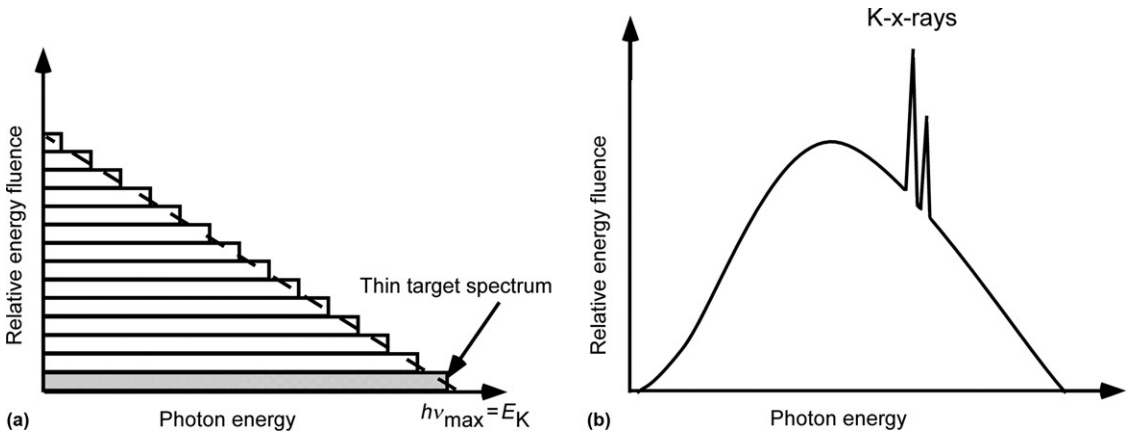

Figure 10 Approximative illustration of the bremsstrahlung spectrum for a thick x-ray target (a) without attenuation or (b) with attenuation in the target and filter and including characteristic x-rays.

where U is the applied voltage. Before the photons will hit the patient, they will be attenuated in the target itself and also in filters positioned between the x-ray tube and the patient, in order to optimize the quality of the image and reduce the absorbed dose to the patient. Low-energy photons are absorbed more, and thus, the bremsstrahlung spectrum will have a curved shape as is Figure 10(b). There will also be a contribution from characteristic x-rays, with energies depending on the target atomic number. Most targets are made of tungsten, and characteristic K x-rays with energies of around 60–70 keV will be included in the spectrum as is indicated in Figure 10(b).

9.01.2.4.3 Radiative stopping power

The total stopping power for inelastic collision with the nucleus is obtained by integrating over all energies, and the following expression is obtained:

$$\left(\frac{S}{\rho}\right)_{\text{rad}} = \alpha r_e^2 Z^2 \frac{N_A}{A}\left(E + m_e c^2\right) B(Z) \qquad [27]$$

The function $B(Z)$ is as mentioned earlier a slowly varying function with energy, and only approximate expressions are published (Bethe and Heitler, 1934). For very low electron energies, $B(Z)$ can be assumed to be constant and eqn [27] becomes

$$\left(\frac{S}{\rho}\right)_{\text{rad}} = \frac{16}{3}\alpha r_e^2 Z^2 \frac{N_A}{A}\left(E + m_e c^2\right) \qquad [28]$$

For higher energies, different expressions for $B(Z)$ have been proposed, and in ICRU Report 35 (1984a), the following expression for the high-energy region is used:

$$\left(\frac{S}{\rho}\right)_{\text{rad}} = \frac{4\alpha r_e^2}{\beta^2} N_A \frac{Z(Z+1)}{A}\left(E + m_e c^2\right) \ \ln\left(183 Z^{-1/3} + 1/18\right) \qquad [29]$$

The factor $Z(Z+1)$ is included instead of Z^2 because bremsstrahlung produced in collisions with electrons has been included. $(S/\rho)_{\text{rad}}$ increases linearly with energy in the MeV region. For energies above 20 MeV, $(S/\rho)_{\text{rad}}$ may be approximated with

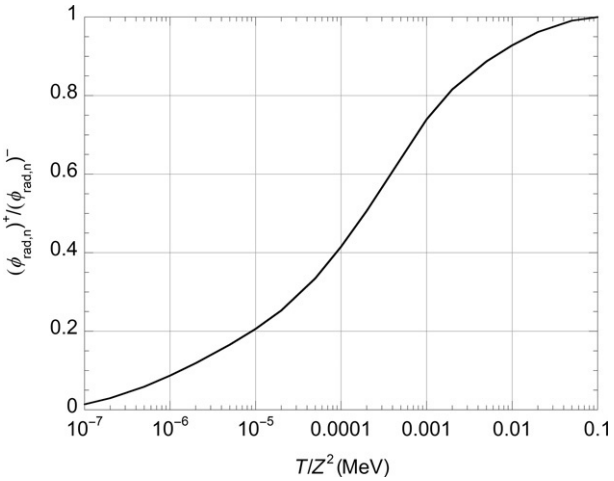

Figure 11 Positron to electron ratios of radiative energy-loss cross sections in the field of the screened nucleus.

$$\left(\frac{S}{\rho}\right)_{\text{rad}} = \frac{E}{X_0} \qquad [30]$$

where X_0 is the radiation length (for the definition, see Section 9.01.2.4.6). $(S/\rho)_{\text{rad}}$ is plotted together with $(S/\rho)_{\text{el}}$ in Figure 6. Positrons and electrons have different radiative stopping powers due to screening of the orbital electrons, which decreases the stopping power for positrons as illustrated in Figure 11.

9.01.2.4.4 Critical energy

From Figure 6, it is clear that collision stopping power is dominant at lower electron energies and radiative stopping power at higher energies. The energy where the radiative stopping power becomes dominant is called the critical energy. An approximate expression for this energy is

$$E_{\text{crit}} = \frac{800}{Z + 1.2} \qquad [31]$$

If $Z=82$, then $E_{\text{crit}}=9.6$ MeV and if $Z=7$, then $E_{\text{crit}}=98$ MeV, which agrees well with the data in Figure 6.

9.01.2.4.5 Radiation yield

The fraction of the energy that is lost through radiation when the electron is totally absorbed is called radiation yield, $Y(E_0)$, where E_0 is the initial kinetic energy of electron. The energy is mainly emitted as bremsstrahlung but can also be obtained from positron-in-flight annihilation and in the form of characteristic x-rays. However, this contribution is often small and neglected. The radiation yield is expressed as

$$Y(E_0) = \frac{1}{E_0}\int_0^{E_0} \frac{S_{\text{rad}}(E)}{S_{\text{tot}}(E)}\, dE \qquad [32]$$

The energy E_{rad} radiated per charged particle is then given by

$$E_{\text{rad}} = E_0 Y(E_0) = \int_0^{E_0} \frac{S_{\text{rad}}(E)}{S_{\text{tot}}(E)} dE \qquad [33]$$

and the energy E_{el} lost through ionization per charged particle is given by

$$E_{\text{el}} = \int_0^{E_0} \frac{S_{\text{el}}(E)}{S_{\text{tot}}(E)} dE \qquad [34]$$

Figure 12 illustrates the radiation yield for water, aluminum, copper, and lead. For example, a 10 MeV electron loses $0.316 \times 10 = 3.16$ MeV as bremsstrahlung in lead but only $0.041 \times 10 = 0.41$ MeV in water when fully absorbed. A practical analytic approach to bremsstrahlung production was developed by Nordell and Brahme (1984), and it was further improved by Svensson and Brahme (1996).

9.01.2.4.6 Radiation length

At high energies where bremsstrahlung is dominating and proportional to energy, the energy loss may be approximated by

$$\frac{dE}{dx} = -kE; \quad \frac{dE}{E} = -k\, dx; \quad E(x) = E_{(0)}e^{-kx} \qquad [35]$$

where k a constant varying with the target material and x is the depth in the material. The radiation energy is then decreasing exponentially for high electron energies. The length over which the electron energy is reduced with a factor of 1/e due to radiation losses is called radiation length, X_R. X_R decreases with increasing atomic number (Figure 13).

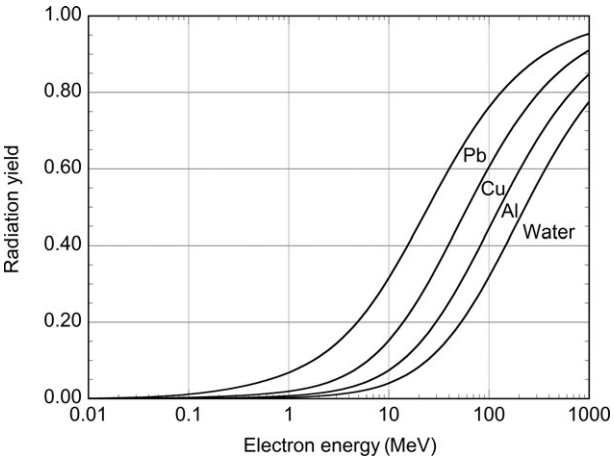

Figure 12 Radiation yield Y_3 for water, aluminum, copper, and lead. Data from NIST Berger et al. (2003).

9.01.2.5 Elastic Scattering

A charged particle can experience Coulomb interaction with a nucleus without losing energy. This process is called elastic scattering. The first experiment to show this was performed by Geiger and Marsden (1909), where α-particles hit a gold foil and were scattered. The results of these experiments made Rutherford (1911) to conclude that most of the mass and positive charge were concentrated in the atomic nucleus, with a radius (1 fm) much smaller than the radius of the atom itself (0.1 nm). Until this experiment was performed, the existing model proposed by Thomson assumed the mass to be uniformly distributed over the whole atom.

9.01.2.5.1 Rutherford scattering

The classical theory to explain the experimental results was derived by Rutherford, and this type of scattering is called Rutherford scattering. To this theory, corrections for spin effects, energy transfer to the nucleus, finite size of the nucleus, and relativistic and quantum effects have to be added to fully explain elastic scattering for other particles and higher energies.

Figure 14 illustrates schematically the scattering of an α-particle with mass m_α and charge ze on a nucleus with the mass M and charge Ze. b is the impact parameter. Rutherford

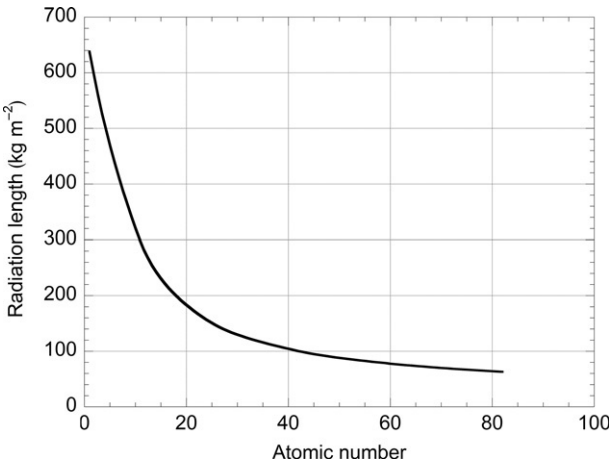

Figure 13 Radiation length X_R, as a function of atomic number.

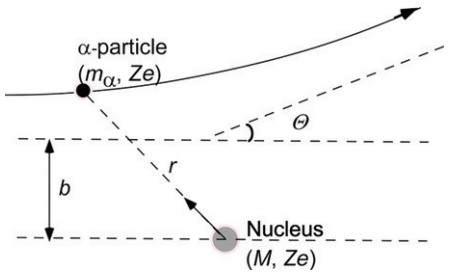

Figure 14 Schematic diagram of the scattering of an α-particle on a nucleus. θ is the final scattering angle.

made in his derivation the following assumptions: (1) Scattering of α-particles on gold nuclei is elastic. (2) Mass of gold nucleus is much larger than the mass of the α-particle. (3) Scattering on electrons is negligible. (4) α-particles do not penetrate the nucleus (no nuclear reaction). (5) Classical mechanics can be used as 5.5 MeV α-particles have the same value of v/c (0.0543) using both classical and relativistic expressions. Using these assumptions, Rutherford could derive the differential cross section

$$\left(\frac{\mathrm{d}\sigma}{\mathrm{d}\Omega}\right)_{\mathrm{Ruth}} = \left(\frac{zZe^2}{16\pi\epsilon_0}\right)^2 \left(\frac{1}{E}\right)^2 \frac{1}{\sin^4\frac{\theta}{2}} \qquad [36]$$

From eqn [36], the following conclusions can be made. The scattering is proportional to the square of the charge z of the incoming particle and the atomic number Z of the target. It is also inversely proportional to the square of the initial kinetic energy E of the α-particle. The variation with scattering angle is inversely proportional to the fourth power of $\sin(\theta/2)$. This implies that scattering is most probable for high atomic numbers, small scattering angles, and low particle energies.

This equation has to be corrected for the screening of the nuclear potential by the orbital electrons, minimum and maximum scattering angles, and the effect of the finite size of the nucleus. Minimum and maximum scattering angles are angles where the deviation from the Coulomb nuclear field becomes significant. These angles are however very small and very large, respectively, corresponding to very large and very small impact parameters, b, which means that the basic Rutherford scattering theory is a good approximation for many situations.

Equation [36] will however get unreasonable results when the scattering angle θ approaches zero as the factor $\sin(\theta/2)$ appears in the denominator. At very small angles, θ, the screening of the nuclear charge by atomic orbital electrons decreases the differential cross section as indicated in Figure 15. For large angles, θ, the finite nuclear size or penetration through the nucleus decreases the differential cross section at angles above 8° for the 5.5 MeV α-particle used in the Geiger–Marsden experiment. Figure 15 shows the Rutherford cross section normalized to include only the factor $1/\sin^4(\theta/2)$. For small angles less than about 0.0001° and large angles around 10°, the Rutherford cross section has been corrected for according to eqns [37] and [38], respectively:

$$\left(\frac{\mathrm{d}\sigma}{\mathrm{d}\Omega}\right)_{\mathrm{Ruth},\,\theta_{\mathrm{min}}} = \left(\frac{\mathrm{d}\sigma}{\mathrm{d}\Omega}\right)_{\mathrm{Ruth}} \frac{16\sin^4\frac{\theta}{2}}{\left(\theta^2+\theta^2_{\mathrm{min}}\right)^2} \qquad [37]$$

$$\left(\frac{d\sigma}{d\Omega}\right)_{\mathrm{Ruth},\,\theta_{\mathrm{max}}} = \left(\frac{d\sigma}{d\Omega}\right)_{\mathrm{Ruth}} \frac{1}{\left(1+\frac{\sin^2\frac{\theta}{2}}{\theta^2_{\mathrm{max}}}\right)^2} \qquad [38]$$

The total cross section is obtained by integrating over all angles. For the interesting scattering angles, the small-angle approximation can be used and then the total cross section is

$$\sigma_{\mathrm{Ruth}} = \left(\frac{zZe^2}{16\epsilon_0}\right)^2 \left(\frac{1}{E}\right)^2 \frac{1}{\theta^2_{\mathrm{min}}} \left\{1 - \frac{1}{1+\left(\frac{\theta_{\mathrm{max}}}{\theta_{\mathrm{min}}}\right)^2}\right\} \qquad [39]$$

Inserting expressions for θ_{min} and θ_{max}, eqn [39] may approximately be expressed as

$$\sigma_{\mathrm{Ruth}} \approx \pi a^2_{\mathrm{TF}} \left\{\frac{2zZe^2}{4\pi\epsilon_0 h v_{\mathrm{i}}}\right\}^2 \qquad [40]$$

where a_{TF} is the Thomas–Fermi atomic radius, h is Planck's constant, and v_{i} is the initial velocity of the α-particle.

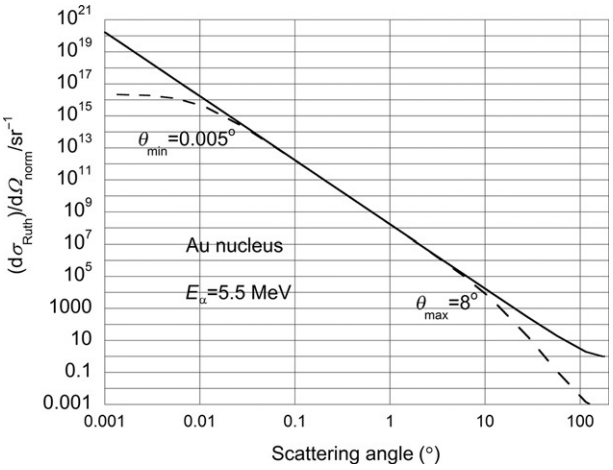

Figure 15 Normalized Rutherford scattering cross section ($1/\sin^4(\theta/2)$) plotted against the scattering angle θ for 5.5 MeV α-particles scattered by a gold nucleus. At low and large scattering angles, data from eqns [37] and [38] are inserted (dashed lines).

9.01.2.5.2 Electron scattering

With electrons as impinging particles, accounts for various parameters have to be included, in particular for high electron energies. Such parameters are electron spin relativistic effects, quantum effects, recoil of the nucleus–nuclear spin and the finite size of the nucleus. These parameters make the derivation of the cross section complex, and different approximative expressions are derived. For low electron energies, it is possible to use the standard Rutherford theory. The Rutherford expression for electrons is then given by

$$\frac{\mathrm{d}\sigma}{\mathrm{d}\Omega} = \left(\frac{Ze^2}{16\pi\epsilon_0}\right)^2 \left(\frac{1}{E}\right)^2 \frac{1}{\sin^4(\theta/2)} \qquad [41]$$

For higher energies, corrections have to be included and Mott (1929, 1932) applied the relativistic theory to include quantum mechanics. McKinley and Feshbach (1948) applied their theory and proposed the expression

$$\frac{\mathrm{d}\sigma}{\mathrm{d}\Omega} = \left(\frac{zZe^2}{16\pi\epsilon_0}\right)^2 \left(\frac{1}{m_{\mathrm{e}}c^2}\right)^2 \left(\frac{1-\beta^2}{\beta^4}\right) \frac{1}{\sin^4(\theta/2)} f(Z,\theta,\beta) \qquad [42]$$

where

$$f(Z,\theta,\beta) = \left[1 - \beta^2\sin^2(\theta/2) + \pi\beta Z\alpha(1 - \sin(\theta/2))\sin(\theta/2)\right] \qquad [43]$$

Comparing classical and quantum theories shows that for heavy elements and intermediate scattering angles, the quantum theory exceeds the classical with more than a factor of 2, while for large angle scattering, the quantum theory can be as little as 10% of the classical one. For very-low-energy particles, the theories will agree.

9.01.2.5.3 Multiple scattering

Equation [39] holds for a single scattering. As elastic scattering is a very common way of interaction, the particles are normally scattered many times even when passing through a thin foil. If the number of scatterings is small, the situation is called plural scattering, and if the number of scatterings is ≥ 20, then this is called multiple scattering, which is easily obtained, often only after a thickness of $10^{-2}\,\mathrm{kg\,m^{-2}}$. All scattering events can be assumed to be independent, except possibly in monocrystalline materials. This will generally result in a Gaussian distribution of scattering angles around the incident particle direction. This simple multiple scattering theory was refined by Molière resulting in a power expansion where the first term is Gaussian followed by single scattering tails. The mean square scattering angle $\overline{\theta^2}$ is calculated from the mean square angle for a single scattering $\overline{\theta_s^2}$. This result is based on the central limit theorem.

The mean square multiple scattering angle for Rutherford scattering is thus obtained by adding the mean square scattering angles for single scatterings:

$$\overline{\theta^2} = n\overline{\theta_s^2} \qquad [44]$$

where n is the number of scattering events. The mean square angle $\overline{\theta^2}$ after passing a mass thickness, ρx, is for heavy charged particles given by

$$\overline{\theta_N^2} = 4\pi \frac{N_A}{A}\rho x\left(\frac{zZe^2}{4\pi\epsilon_0 E}\right)^2 \ln\left(183Z^{-1/3}\right) \qquad [45]$$

For electrons, the corresponding equation is

$$\overline{\theta_e^2} = 16\pi\rho x \frac{N_A r_e^2 Z(Z+1)\left(1-\beta^2\right)}{A\beta^4} \ln\left(183Z^{-1/3}\right) \qquad [46]$$

Equations [45] and [46] will give a linear increase of $\overline{\theta^2}$ with increasing thickness, but this holds only for small thicknesses as discussed in Section 9.01.5.4.

The change in mean square scattering angle with thickness is given by the mass scattering power, T/ρ, defined as

$$\frac{T}{\rho} = \frac{\mathrm{d}\overline{\theta^2}}{\mathrm{d}(\rho x)} \qquad [47]$$

For electrons, T/ρ is more accurately given by

$$\frac{T}{\rho} = 4\pi\frac{N_A}{A}\frac{r_e^2 Z(Z+1)\left(1-\beta^2\right)}{\beta^4}\left\{\ln\left(1+\frac{\theta_{max}^2}{\theta_{min}^2}\right) - 1 + \left(1+\frac{\theta_{max}^2}{\theta_{min}^2}\right)^{-1}\right\} \qquad [48]$$

Figure 16 illustrates the mass scattering power T/ρ, as a function of electron energies up to 10 MeV for PMMA, copper, tin, and lead. The nearly linear Z-dependence and strong energy dependence $(1/E^2)$ are demonstrated. A similar expression for light ions was given by Kempe and Brahme (2010). Compare also with Hollmark et al. (2008) where data unfortunately are miscalculated.

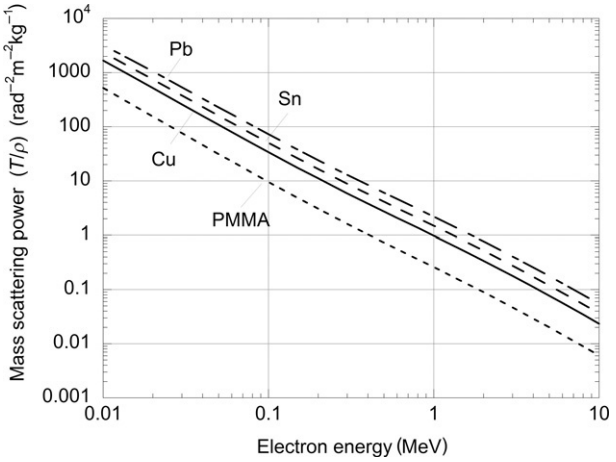

Figure 16 Mass scattering power T/ρ as a function of electron energy for PMMA, Cu, Sn, and, Pb.

9.01.2.5.4 Fermi–Eyges pencil beam model

The transport of an electron pencil beam through matter has been described by the Fermi–Eyges transport model (Eyges, 1948; Fermi, 1940). Assume that the electrons are multiply scattered in small angles and that the Molière multiple scattering theory is applicable. Then, the angular distribution at a depth, z, in the matter is given by

$$P(z,\theta) = \frac{1}{\pi\overline{\theta^2}(z)}\mathrm{e}^{-\frac{\theta^2}{\overline{\theta^2}(z)}} \qquad [49]$$

where $\overline{\theta^2}(z)$ is the mean square scattering angle at depth z. The value of $\overline{\theta^2}(z)$ can be calculated using the mass scattering power T/ρ with the relation

$$\overline{\theta^2}(z) = \overline{\theta^2}(0) + (T/\rho)\rho z \qquad [50]$$

where $\overline{\theta^2}(0)$ is the mean square scattering angle at depth $z=0$. For example, if assuming $\overline{\theta^2}(0) = 0$, $\overline{\theta^2}(z)$ will for 5 MeV electrons and a thickness of $\rho z = 1.0\,\mathrm{kg\,m^{-2}}$ be 26° for water and 76° for Pb. Increasing the thickness to $10\,\mathrm{kg\,m^{-2}}$ gives instead 96° for water and 241° for Pb. These results are not realistic. The simple calculations do not take into consideration the change in T/ρ with depth and thus decrease in energy. This will increase $\overline{\theta^2}(z)$ even faster. Another more important factor is that the angular distribution will after some depth reach an equilibrium as there are both inscatter and outscatter. This diffusion equilibrium has a value of $\overline{\theta^2}$ close to $0.65\,\mathrm{rad^2}$ or a mean scattering angle of 46°.

Corresponding to the angular distribution, there will also be a radial distribution of the electrons:

$$P(z,r) = \frac{1}{\pi\overline{r^2}(z)}\mathrm{e}^{-\frac{r^2}{\overline{r^2}(z)}} \qquad [51]$$

where $\overline{r^2}(z)$ is the mean square radius at depth $z=0$. $\overline{r^2}(z)$ may be calculated using the relation

$$\overline{r^2}(z) = \overline{r^2}(0) + 2\overline{r\theta}(\rho z) + \overline{\theta^2}(0)(\rho z)^2 + (T/\rho)\rho^3 z^3/3 \qquad [52]$$

where $\overline{r^2}(0)$ is the mean square radius at depth $z=0$, that is, the radius of the incoming electron beam (Brahme, 1975). These

equations have been valuable for calculating and understanding the transport of both electrons and heavy charged particles in, for example, radiotherapy, and are treated in detail in Chapter 9.03.

9.01.2.6 Ranges and Stopping Power

9.01.2.6.1 Stopping power

The total stopping power is obtained by adding the stopping power for inelastic collisions, radiative interactions, and nuclear interactions:

$$\frac{S_{tot}}{\rho} = \frac{S_{el}}{\rho} + \frac{S_{rad}}{\rho} + \frac{S_{nucl}}{\rho} \qquad [53]$$

For heavy charged particles, only S_{el}/ρ and S_{nucl}/ρ are of interest, and S_{nucl}/ρ will have an impact on the total stopping power only for energies below around 1 MeV for α-particles and 0.1 MeV for protons as is indicated in Figure 4. For electrons, only S_{el}/ρ and S_{rad}/ρ will be of interest, where S_{el}/ρ will dominate at low energies and S_{rad}/ρ at high energies as discussed and shown in Figure 6.

The uncertainties of the collision stopping power for electrons tabulated in ICRU Report 37 (ICRU, 1984b) are estimated to be 1–2% for energies above 100 keV. Between 10 and 100 keV, they are estimated to be 2–3% in low Z-materials and 5–10% in high Z-materials. The uncertainty of the radiative stopping power is estimated to be around 2% above 50 MeV. Between 2 and 50 MeV, they are estimated to be 2–5% and below 2 MeV around 5%. These uncertainties are estimated to correspond to a significance of 90%.

9.01.2.6.2 Ranges

From a macroscopic point of view, it is of interest to determine the transmission and range of charged particles in a medium. This depends on the interaction processes and their cross sections. Both energy losses as inelastic collisions and elastic scattering processes are important. There is a difference in transmission between heavy charged particles like protons and electrons (Figure 1). A heavy charged particle will undergo several very-small-angle scatterings and have more or less a linear path with many very small energy losses ($\Delta E_{max} = 4m_e E/M$). Electrons, on the other hand, are deflected significantly and can lose up to half of its energy in an inelastic collision or even all of its energy in a bremsstrahlung process.

This will imply that not all particles will have the same range, in particular for electrons but to a smaller extent also for heavy charged particles. Due to this, several definitions of 'ranges' have been proposed, and it is important to specify which range one is referring to. The total distance a particle has traveled along its trajectory is often called the path length, while the path length projected onto the direction of the incident particle is called range.

However, ICRU has introduced a concept called r_{csda}, which is more a path length than a range according to the definition mentioned. The CSDA range assumes that the particles lose energy continuously and that is why this path length is called the continuous slowing down approximation range, r_{csda}, defined as

$$r_{csda} = \int_0^{E_0} \frac{dE}{S_{tot}(E)} \qquad [54]$$

where E_0 is the initial kinetic energy of the particle and $S_{tot}(E)$ is the total stopping power.

9.01.2.6.3 Heavy charged particles

For heavy charged particles, r_{csda} generally is a good approximation for the projected range. For low particle energies, there will be a difference as shown in Figure 17 where r_{csda} is compared with the projected range for protons and α-particles. The difference is larger for high atomic numbers where the scattering power is higher. The r_{csda} range for heavy charged

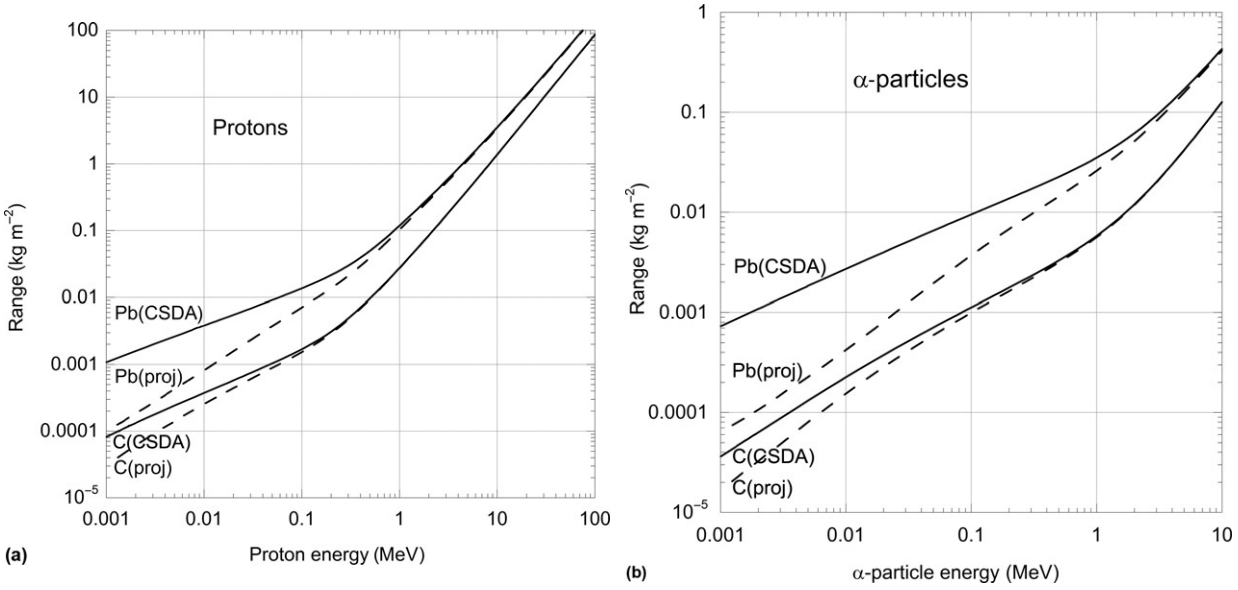

Figure 17 Comparison of the r_{csda} and the projected range for protons and α-particles.

particles can then be obtained using the relations for stopping power:

$$r_{\text{csda}} = \frac{2MA}{Z4\pi N_A r_e^2 m_e c^4 z^2} \int_0^{E_0} \frac{\frac{E}{M}\,\mathrm{d}\left(\frac{E}{M}\right)}{\ln\left(\frac{4m_e}{I}\,\frac{E}{M}\right)} \qquad [55]$$

where M is the particle mass, A is the mass number, Z is the atomic number of the material, N_A is the Avogadro constant, r_e is the classical electron radius, c is the velocity of light in vacuum, z is the charge of the particle, and E is the kinetic energy of the particle. The range of protons and α-particles can be calculated with the NIST programs PSTAR and ASTAR available at the NIST web page. Figure 18 shows some calculated ranges using these programs. As expected, the ranges are increasing with increasing atomic number as higher atomic numbers have lower stopping power values and the scattering power has in this situation less importance (compare with that of electrons discussed later). For determining the range for other heavy charged particles, it is possible to use the scaling law given in eqn [56]. This relation is a good approximation except for very low energies:

$$r_{z,M} = \frac{1}{z^2}\,\frac{M}{m_p} r_p \qquad [56]$$

$r_{z,M}$ is the range of a particle with charge z and mass M and r_p is the range of a proton (charge = 1 and mass = m_p) with the same velocity.

Another expression that can be used for calculating the range for α-particles is the empirical relation

$$r_\alpha = \frac{(E)^{3/2} A^{1/2} 10^{-3}}{\rho}\,\text{m if } \rho \text{ in kg m}^{-3} \qquad [57]$$

where A is the mass number and E the kinetic energy. An α-particle with an energy of 5.5 MeV will have a range in air of 0.035 m or 3.5 cm. This illustrates the short range for α-particles even in air.

The variation of fluence with depth for heavy charged particles will have a rather straight plateau before it ends with a fast gradient. Figure 19 shows some proton depth dose distributions in soft tissue for proton energies between 100 and 1000 MeV. The fluence is more or less flat, but there is a variation in absorbed dose with depth, due mainly to the change in stopping power with depth, which first increases slowly and ends with a fast increase when the protons approaches very low energy values. This will give rise to a sharp peak, called the Bragg peak. This peak can be of interest in radiotherapy with light ions, in particular for ions heavier than protons, due to more nuclear reactions, giving rise to a

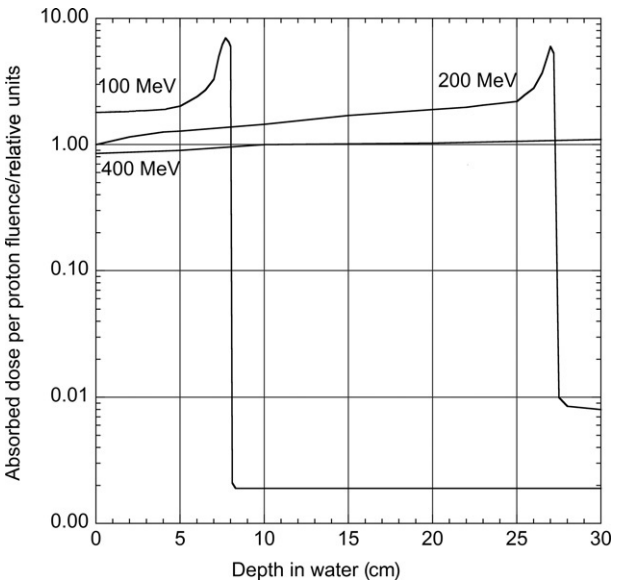

Figure 19 Variation of depth dose in tissue for protons with energies between 100 and 1000 MeV. Adapted from ICRP (1973).

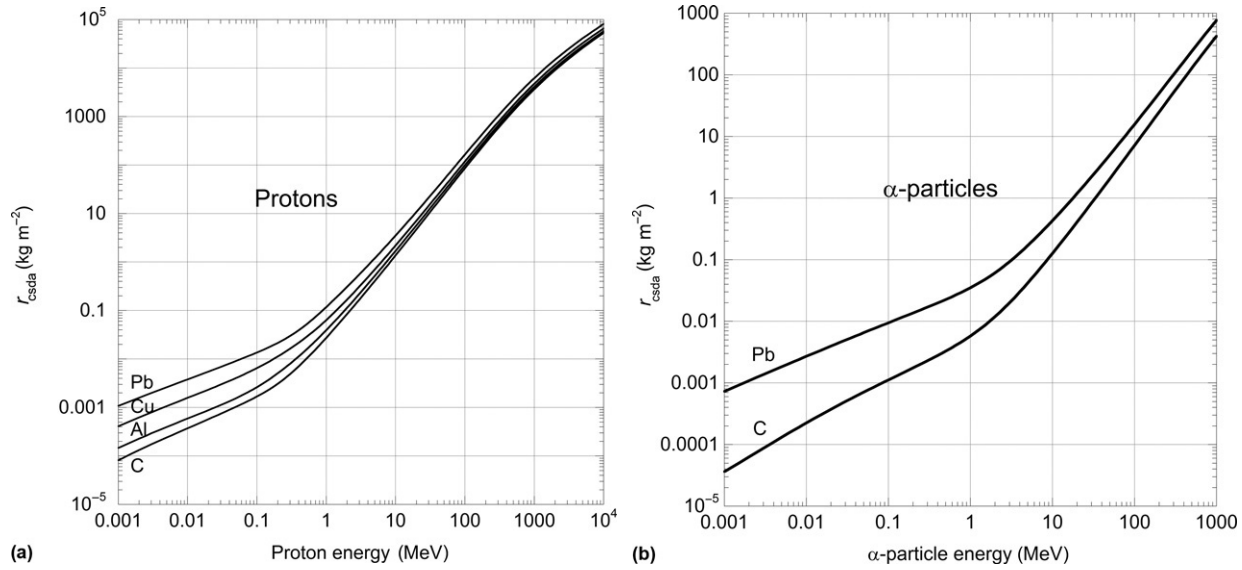

Figure 18 r_{csda} for (a) protons (carbon, aluminum, copper and lead) and (b) α-particles (carbon and lead).

higher LET in the peak. Figure 19 also indicates that to reach more than 20 cm into the body, 200 MeV protons are needed.

Even if the fluence is nearly constant over most of the particle range, the energy decreases and the energy fluence will continuously decrease. As the energy losses are small, the energy distribution is narrow and the energy straggling is small as well as the range straggling.

Kempe and Brahme (2008, 2010) had developed analytic expressions for the variation of the mean energy and the fluence with depth for light-ion beams. These expressions agree well with the data obtained through Monte Carlo calculations and could be of interest for fast calculations needed in clinical treatment planning.

9.01.2.6.4 Electrons and positrons

As mentioned earlier, the variation in range is large for electrons and the difference between the path length and the projected range is often significant. Figure 20 shows the ratio between experimentally projected ranges r_p and r_{csda} for carbon, aluminum, copper, silver, and uranium for electron energies up to 12 MeV. For high atomic numbers and low energies, the ratio is below 0.5, while for low atomic numbers and high energies, the ratio is even over 1.0, due to range straggling. This shows that for practical situations, r_{csda} often largely overestimates the projected range and experimental-obtained ranges are more useful, at least for radiation protection applications.

The variation of electron fluence for primary electrons with depth is plotted in Figure 21 for water and tantalum for 5 and 10 MeV electrons. For electrons, scattering and partly large energy losses reduce the fluence directly at small depths. Note that tantalum has a lower collision stopping power than water, but due to the higher atomic number of tantalum, it a has a much higher scattering power and this has a large impact on the depth fluence distribution. The curves are calculated for the primary electrons only. There will also be secondary electrons produced that will be added to the fluence. The contribution from these electrons depends on energy and material but can be up to 20% of the total fluence in water.

The discussion has so far been directed to fluence of plane-parallel monoenergetic electrons. With radioactive β sources, there are two factors that will influence the transmission. One is that the β-particles are emitted with an energy distribution. The other factor is that the β-particles are emitted isotropically. These two factors will result in a nearly exponential decrease of the fluence. This means that the fluence can be calculated using empirical-determined absorption coefficients. The mass absorption coefficient is varying with atomic number and maximal β-particle energy. As they are empirically obtained, different values and relations are published. Most measurements of β-particles have been made with aluminum as absorber, and for aluminum, a commonly used expression is

$$\frac{\beta}{\rho} = \frac{1.7}{E_{max}^{1.4}}\,\mathrm{m^2\,kg^{-1}} \qquad [58]$$

where E_{max} is expressed in MeV.

The range of β-particles does not differ that much from monoenergetic electrons with the same energy as E_{max}, as there are some β-particles with maximum energy irradiated in the forward direction. There are several empirical relations for determining β-particle ranges. These are mainly linear in energy with two parameters:

$$r_\beta = AE_{max} - B \qquad [59]$$

where A has a value close to 0.5 and B is a small correction factor.

Positrons have slight different interaction cross sections as discussed. This will also result in a small difference in range. As the cross section for positrons is both larger and smaller than the cross section for electrons over the energy range, the difference in range will not be that large as shown in Figure 22 where the ratio of ranges for positrons to electrons is plotted. The results reflect the variation in cross sections for the stopping powers of electrons and positrons with a smaller stopping

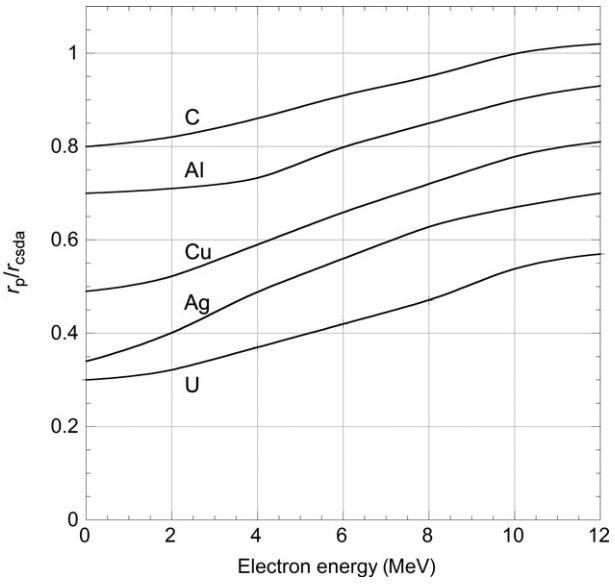

Figure 20 Ratio of the projected range r_p and r_{csda} for carbon, aluminum, copper, silver, and uranium for electrons with energies up to 12 MeV.

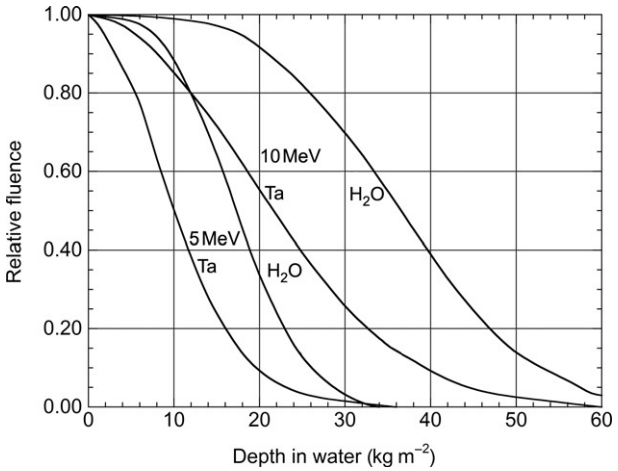

Figure 21 Variation of the planar electron fluence with depth in water and tantalum for 5 and 10 MeV electrons.

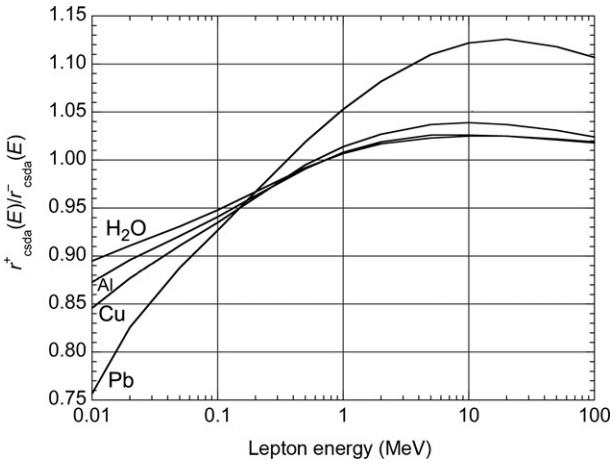

Figure 22 Ratio of r_{csda} for positrons and electrons for water, aluminum, copper and lead.

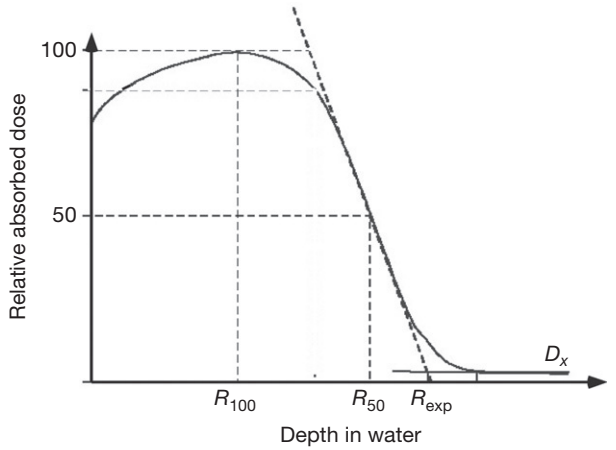

Figure 23 Electron depth dose curve with definitions according to ICRU (1984a). R_p is the extrapolated range R_{exp} in the figure.

power at higher energies for positrons, giving large ranges, but higher at low energies giving small ranges compared with electrons.

9.01.2.6.5 Radiotherapy beams

In radiotherapy, it is important to have a high accuracy and an agreement of the definitions. Figure 23 illustrates an electron depth dose distribution and the range definitions proposed by ICRU (1984b). R_{50} is the depth where the absorbed dose has decreased to half of its maximum value at R_{100}. This value is used as a measure of the beam quality and shall be used instead of the nominal accelerating energy when determining dosimetry parameters. R_p is related to the electron energy distribution. A narrow electron energy distribution impinging on the phantom will for a certain energy result in a high dose gradient, and R_p gives an indication of this dose gradient. It also is an indication of the maximal range.

The depth dose distribution starts with a buildup region, which is mainly a result of the increase in fluence due to multiple scattering, which increases the angular distribution and thus the fluence. There is also a production of secondary electrons as mentioned earlier. At the high energies normally

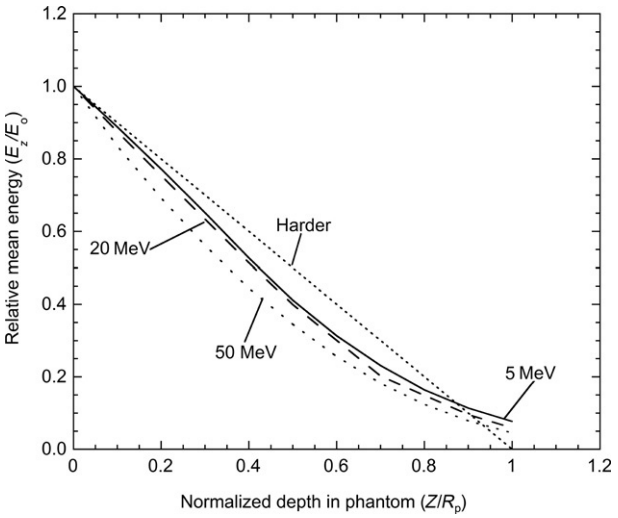

Figure 24 Variation of electron energy with depth using eqn [60] by Brahme and eqn [61] by Harder.

used in radiotherapy, there is also a contribution from bremsstrahlung photons, produced not only in the treatment gantry but also in the phantom. This contribution is seen as the tail after the maximum range of the electrons. R_{50} increases with increasing electron energy, and Brahme and Svensson (1976) have proposed a linear relation between R_{50} and the mean energy at phantom surface, $\overline{E}_0 = 2.33R_{50}$, which is in good agreement with measurements for many electron accelerators. For dosimetry reasons, it is also important to know the electron energy distribution at different depths. This energy distribution is not Gaussian but slightly skewed towards lower energies. This distribution, that is, called Vavilov or Landau distribution, results in that the mean energy $\overline{E}(z)$ and the most probable energy $E_p(z)$ at depth z differ. The electron energy distribution is often calculated using Monte Carlo methods, but sometimes, it may be of interest with just the mean energy. Brahme (1975) has proposed an expression for the variation of mean energy with depth in water, which gives a good agreement with Monte Carlo-calculated values in the first half of the depth dose curve:

$$\overline{E}(z) = \overline{E}_0 - S_{tot,0}\frac{1 - e^{S_{rad,0}z/E_0}}{S_{rad,0}z/E_0} \qquad [60]$$

Harder (1965) had earlier proposed a linear relationship between energy and depth:

$$E_p(z) = E_{p,0}\left(1 - \frac{z}{R_p}\right) \qquad [61]$$

This equation was primarily proposed to hold for the mean energy, but it fits better to the most probable energy. Figure 24 illustrates the variation of energy with depth according to the Brahme and Harder relations. For ions, a similar relation is derived by Kempe and Brahme (2008). The mean energy is here given as

$$E_{(z)} = \overline{E}_0\left(1 - \frac{kS_0}{\overline{E}_0}z\right)^{1/k} \qquad [62]$$

where the dimensionless transport parameter

$$k = \frac{\bar{E}_0}{R_0 S_0} \quad [63]$$

expresses the ratio of the mean rate of energy loss over the whole slowing down range, $\bar{E}_0/R_0$, to the value at the phantom surface S_0. Interestingly, the first two terms in the expansion of eqn [62] are similar to eqn [61] with R_p replaced by R_0.

9.01.3 Photons

9.01.3.1 Introduction to Photon Interaction

Photon interaction with matter involves mainly the production of secondary energetic charged particles like leptons (electrons and positrons). It is these leptons that deposit energy in the material by ionizations and excitations, and the ionization in the primary interaction process is often neglected, when calculating absorbed dose. For example, a 100 keV electron may produce around 3000 ionizations as compared with the one produced by the photon emitting the electron. The energy transferred to the leptons is sometimes considered as absorbed energy, and the energy of the secondary photons as scattered energy. The most important photon interaction processes can be described as a function of the interaction target (Table 1). The types of interaction for photons that are normally included in tabulated values of the mass attenuation coefficient, μ/ρ, are photoelectric effect, coherent scattering, incoherent scattering, and pair production in the electron and the nuclear field. For some reasons, the nuclear cross section is normally not included, even if it for some energies can contribute to some percent of the total cross section.

The different interaction probabilities are generally given in form of cross sections with the unit m^2 per (atom, nucleus, or electron). The mass attenuation coefficient is related to the atomic cross section according to the relation

$$\frac{\mu}{\rho} = \frac{N_A}{M} \sum_J \sigma_J \quad [64]$$

where σ_J is the component cross section relating to interaction type J, N_A is the Avogadro constant, and M is the molar mass.

The mass attenuation coefficient is obtained by adding the cross sections of the different interaction types. μ/ρ may thus be expressed, if the contribution from photonuclear processes are included, as

$$\frac{\mu}{\rho} = \frac{\tau}{\rho} + \frac{\sigma_{coh}}{\rho} + \frac{\sigma_{incoh}}{\rho} + \frac{\kappa_n}{\rho} + \frac{\kappa_e}{\rho} + \frac{\sigma_{pn}}{\rho} \quad [65]$$

where τ/ρ is the mass cross section for photoelectric effect, σ_{coh}/ρ for the coherent (Rayleigh) scattering, σ_{incoh}/ρ for the incoherent scattering (Compton effect), κ_n/ρ for pair production in the nuclear field, κ_e/ρ for pair production in the electron field and σ_{pn}/ρ is the photonuclear mass cross section. The use of the mass attenuation coefficient μ/ρ instead of the linear attenuation coefficient, μ, is practical for compilation purposes, and it is always μ/ρ that is found in the tables.

Consider a narrow photon beam hitting a material (Figure 25). Some of the photons will transmit the material without interaction. Other photons will interact, and in the interaction of the photons, secondary or scattered photons, and secondary electrons will be produced. These interacting photons are called attenuated. The probability that a photon is interacting in a thin layer $d(\rho x)$ of the material is given

Table 1 Overview of the different photon interaction possibilities

Target	*Effect of interaction*	*Name of interaction*	*Notation*
Atom	Complete absorption	Photoelectric effect	τ
	Coherent scattering	Rayleigh scattering	σ_{coh}
Atomic electron	Incoherent scattering	Compton effect	σ_{incoh}
	Complete absorption	Pair production in the electron field	κ_e
	Elastic scattering	Thomson scattering	σ_{Th}
Nucleus	Complete absorption	Pair production in the nuclear field	κ_n
	Complete absorption	Photonuclear	σ_{pn}
	Complete absorption	Production of mesons	σ_m

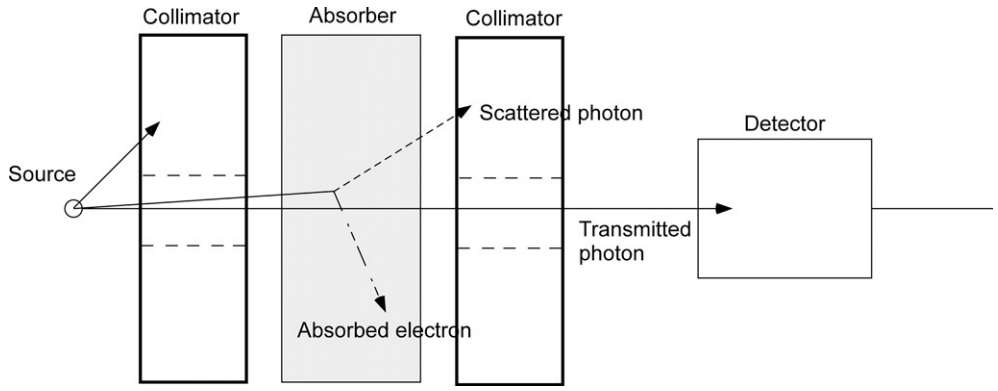

Figure 25 Schematic illustration of transport of photons through an absorber.

by $(\mu/\rho)\mathrm{d}(\rho x)$ where μ/ρ is the mass attenuation coefficient. Integrating the fractional reduction of the beam fluence in a thin layer gives the transmitted fluence through a thickness ρx as

$$\Phi_{\rho x,\,\mathrm{n}} = \Phi_0\, \mathrm{e}^{-(\mu/\rho)(\rho x)} \qquad [66]$$

This relation holds for narrow beams that are well collimated both before and after the absorbing material, and thus, only transmitted primary photons are included. In most situations, there is also a contribution from secondary photons, mainly incoherent scattered photons, but also annihilation photons and characteristic (fluorescence) x-rays. Whether the coherent scattered photons, with the same energy as the primary ones, shall be considered as secondary or not can depend on the geometry. The contribution from secondary photons is often included by multiplying the transmitted fluence with a *build-up factor*, B, which is the ratio of the total transmitted fluence to the primary fluence:

$$\Phi_{\rho x,\,b} = B\Phi_0\, \mathrm{e}^{-(\mu/\rho)(\rho x)} \qquad [67]$$

The mass attenuation coefficient of a compound is obtained by treating the compound as consisting of independent atoms, neglecting any molecular binding energies. Thus,

$$\left(\frac{\mu}{\rho}\right)_{\mathrm{comp}} = w_1\left(\frac{\mu}{\rho}\right)_1 + w_2\left(\frac{\mu}{\rho}\right)_2 + \cdots + w_j\left(\frac{\mu}{\rho}\right)_j \qquad [68]$$

where w is the mass fraction of each atomic material in the compound. This relation is sometimes called the Bragg relation. This is a good approximation except for very low photon energies.

The different interaction processes are treated in the following sections, where both the probability for the interaction process and the energy and angular distributions of the secondary photons and leptons are discussed.

9.01.3.2 Photoelectric Effect

For low photon energies, below approximately 100 keV, the photoelectric effect is the dominating interaction process in medium- and high-atomic-number materials. In a photoelectric process, the photon is totally absorbed by the atom and the energy is transferred to an atomic electron (Figure 26). The electron cannot be a free electron, as this will not fulfill the energy and momentum relations. These relations give

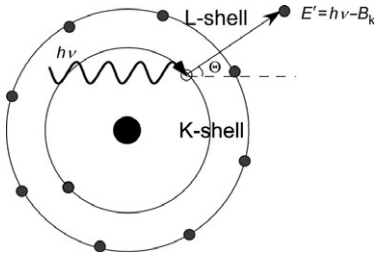

Figure 26 Schematic description of a photoelectric effect. A photon with energy $h\nu$ transfers its energy to an atomic electron, which is emitted with the energy $h\nu - B_{\mathrm{K,L,\ldots}}$.

$$\mathrm{p}_\gamma = \mathrm{p}'_\mathrm{e} + \mathrm{p}'_\mathrm{i}; \quad h\nu = B_\mathrm{nj} + E'_\mathrm{e} + E'_\mathrm{i} \qquad [69]$$

where γ, e, and i represent the incoming photon, the emitted photoelectron, and the recoil ion. B_{nj} is the binding energy of the electron in shell n and subshell j. Assume now that the electron is free. Then, $p'_\mathrm{i} = E'_\mathrm{i} = B_{nj} = 0$. This gives

$$p_\gamma c = h\nu = p'_\mathrm{e}c = \sqrt{\left(E'_e\right)^2 + 2m_e c^2 E'_e} > E'_e \qquad [70]$$

This does not agree with the energy conservation rules for interaction with a free electron where $h\nu = E'_\mathrm{e}$ should hold.

The electron is often a K-electron, as these are the most tightly bound electrons. About 80% of the photoelectric interactions take place in the K-shell, nearly independent of the atomic number.

The energy and momentum relations also give that

$$h\nu_{\mathrm{min},\,nj} = B_{nj}\left[1 + \frac{B_{nj}}{2M_\mathrm{x}c^2}\right] \qquad [71]$$

As $B_{nj} \ll M_\mathrm{x}c^2$, this implies that the threshold energy for the photon is equal to the binding energies in the different shells. The electron kinetic energy will become

$$E' = h\nu - B_{nj} \qquad [72]$$

9.01.3.2.1 Total cross section

The probability for a photoelectric effect is based approximately on calculations for a K-electron using an unscreened Coulomb potential, for energies not too close to the binding energies. Correction factors are then applied to take into consideration the effect of the K-edge and the contributions from L-, M-,... electrons and the screened potential. For low photon energies, Heitler (1954) obtained the relation

$$\tau_K = 4(2)^{1/2}\alpha^4\sigma_0\frac{Z^5(m_\mathrm{e}c^2)^{7/2}}{(h\nu)^{7/2}} \qquad [73]$$

where α is the fine structure constant 1/137 and σ_0 is the Thomson scattering cross section:

$$\sigma_0 = \frac{8}{3}\pi r_\mathrm{e}^2 \qquad [74]$$

At high energies, relativistic corrections must be included and an expression obtained by Sauter is

$$\tau_\mathrm{K} = \sigma_0\frac{3}{2}\alpha^4\frac{Z^5 m_\mathrm{e}c^2}{(h\nu)} \qquad [75]$$

As is obvious from the equations for the cross sections, there is a high dependence on both the atomic number, Z, and the photon energy, $h\nu$. At low energies where the photoelectric effect is dominant, the variation with energy is close to $(h\nu)^{-3}$. At high photon energies, the variation with energy has decreased to $(h\nu)^{-1}$. The variation with atomic number is, after corrections, changing with energy between Z^4 at low energies and Z^5 at very high energies.

The aforementioned cross sections hold for the photoelectric effect in the K-shell. The interactions with outer shells must be added, and if the photon energy is lower than the binding energy of a specific shell, then the effect can only be applied to outer shells. Figure 27 shows the relation $\tau_{\mathrm{shell}}/\tau$ for the K-, L_1-,

and M_1-shells as a function of atomic number for photon energies close to the binding energy. An approximate expression for the relation τ/τ_K is given by Hubbell (1969):

$$\tau/\tau_K = 1 + 0.01481(\ln Z)^2 - 0.00079(\ln Z)^3 \qquad [76]$$

Corrections to the aforementioned equations have also to be applied due to the screening effect, which reduces the cross section with a percentage that is rather independent of the photon energy and around 2% for the K-shell but up to 30% for the L-shells.

Close to the energy of the electron binding energies, there is a large discontinuous change in the cross section because if the energy is just below, for example, the binding energy of the K-shell, then no K-electrons can be expelled, but with an energy just above the binding energy, this is possible. Tables of photon cross sections always have two lines corresponding to the binding energy. One is the value of the cross section just below the binding energy, and one is the value of the cross section just above the binding energy. Figure 28 illustrates the photoelectric cross section for Pb and water for energies between 0.01 and 100 MeV. The discontinuities at the absorption edges for the K- and the L-shells for Pb are clearly expressed. For water, the binding energy is lower than 10 keV.

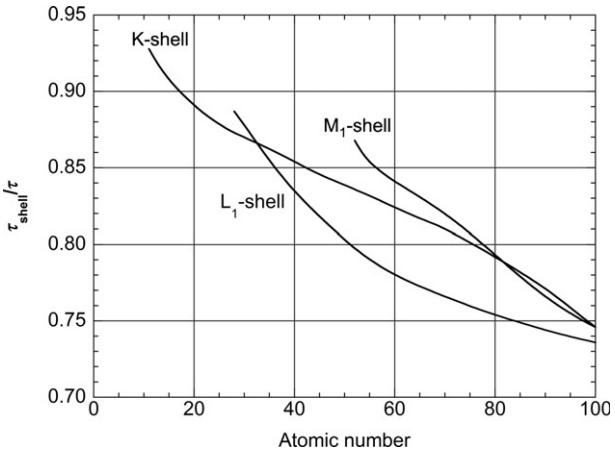

Figure 27 Ratio of the cross section for photoelectric effect in different subshells to the total cross section.

9.01.3.2.2 Angular distribution

For calculations of the transport of the emitted photoelectrons, it is of interest to know their angular distribution. For low photon energies, Sauter (Brysk and Zerby, 1968) proposed, for interactions in the K-shell, a relation for the differential cross section in scattering into the solid angle at θ:

$$d\tau/d\Omega = C \sin^2\theta \left(E'_{ph} - (p/m_e c^2)\cos\theta\right)^{-4} \qquad [77]$$

where C is a normalization constant, E'_{ph} is the electron energy expressed in electron rest masses, and p is the electron momentum. This relation gives a symmetrical distribution around 90°. For higher energies, the angular distribution is more forward-directed, and the angular distribution is given by (Brysk and Zerby, 1968)

$$\frac{d\tau}{d\Omega} = C \sin^2\theta \left(E'_{ph} - (p/m_e c^2)\cos\theta\right)^{-4} \times \left[1 - \frac{1}{2}\left(E'_{ph} - 1\right)\left(2 - E'_{ph}\right)\left(E'_{ph} - (p/m_e c^2)\cos\theta\right)\right] \qquad [78]$$

Figure 29 shows the normalized angular distribution for some photon energies.

9.01.3.2.3 Auger electrons and characteristic x-rays

The electron vacancy produced in a photoelectric effect is followed by an electron from a higher-level electron shell replacing the vacancy. The new vacancy is then replaced by new electrons from outer shells and a cascade of electron

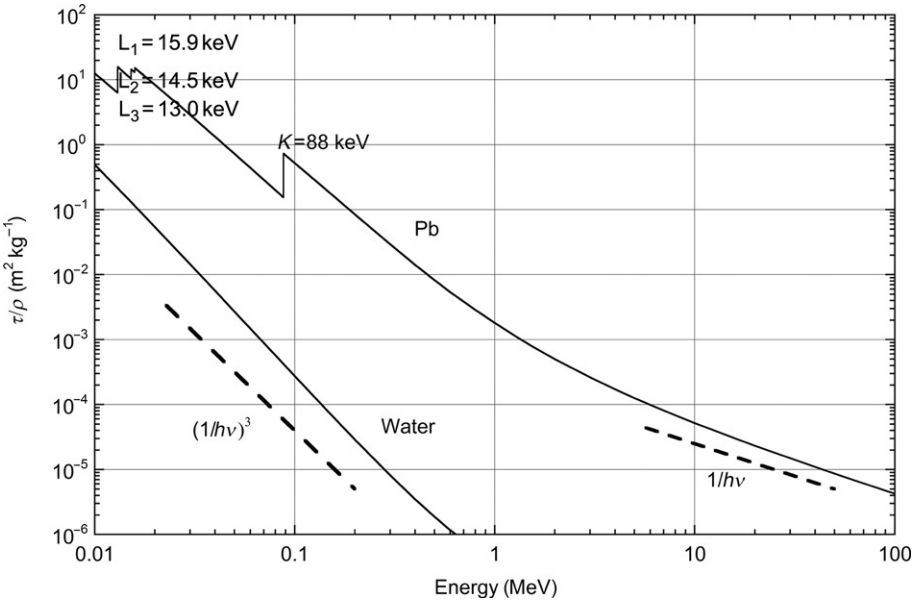

Figure 28 Cross section for photoelectric effect in water and lead as a function of photon energy.

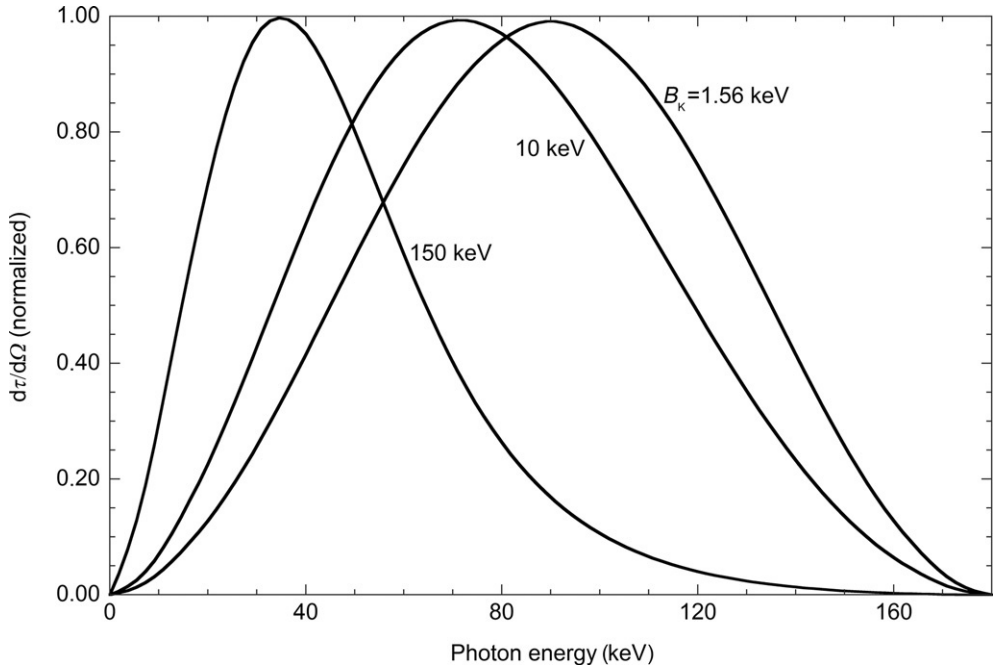

Figure 29 Angular distribution of photoelectrons from the K-shell of aluminum for various incident energies.

vacancies is possible until a 'free' electron will neutralize the atom. The transition energies obtained are emitted either as characteristic x-rays or as electrons. These electrons are in general called Auger electrons and, if the transitions are between subshells, Coster–Kronig electrons.

9.01.3.2.4 Fluorescence yield

The probability that the vacancy results in characteristic x-rays is called the *fluorescent yield*, ω. Previously, the characteristic x-rays had different notations according to a system developed by M. Siegbahn, a Swedish physicist. For example, if the vacancy is in the K-shell and the electron comes from the L3-shell, the x-ray was called a $K_{\alpha 1}$ x-ray in the Siegbahn notation. Lately, the International Union of Pure and Applied Chemistry has proposed a new nomenclature by just indicating the shells. In this nomenclature, the x-ray is called x_{K-L3}. The energy of the characteristic x-rays is the difference between the binding energy of the two electron shells involved. Thus, an x_{K-L3} x-ray will have the energy $B_K - B_{L3}$. As these energies are typical for a specific atomic number, the energy of the characteristic x-rays can be used to identify the atomic composition of unknown material. The energies and the fluorescent yields of different characteristic x-rays can, for example, be found in the Table of Radioactive Isotopes (Browne and Firestone, 1986).

The fluorescent yield, ω, increases with atomic number and is low for atomic numbers <10, typical in tissue, but high in, for example, Pb. Figure 30 shows the variation of ω with atomic number for the K- and the L_2-shell.

9.01.3.2.5 Auger electron yield

As the emission of Auger electrons is an alternative to the emission of characteristic x-rays, the probability is $1-\omega$. There are a lot of different possible combinations. A primary vacancy in the K-shell can, for example, be replaced by an

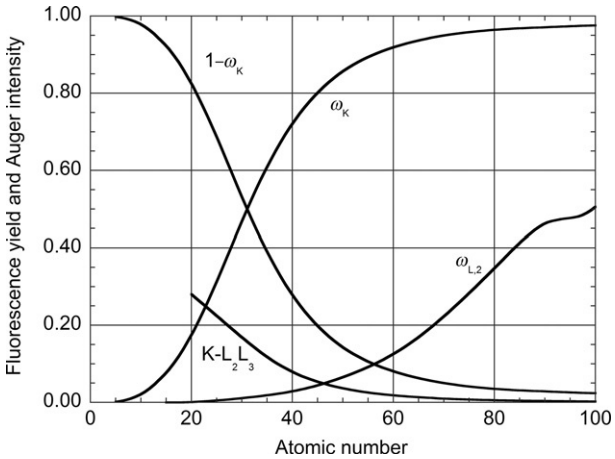

Figure 30 Fluorescence yields for ω_K and ω_{L2} as a function of atomic number. The probability for Auger effect in K-shell is also included together with the probability for only K–L_2L_3 transition. Data taken from Browne and Firestone (1986).

electron from one of the L-subshells. The transition energy can be used to emit an electron in any L-subshell or in a higher-order shell. In the Tables of Radioactive Isotopes, Auger electron intensities are tabulated, and as an example, 56 different combinations are listed for the atom Pb. Figure 30 illustrates the probability for emission of a K–L_2L_3 Auger electron, which is the most probable transition, as a function of atomic number.

The energy of the Auger electrons is corresponding to the energy of the characteristic x-rays equal to the difference in the binding energies of the involved electrons. Thus, the energy of a K–L_2L_3 electron is $B_K - B_{L_2} - B_{L_3}$.

9.01.3.3 Coherent and Incoherent Scattering

A low-energy photon can be scattered by a loosely bound or 'free' electron. Thomson (1933) described this with a classical theory, where the electron starts to oscillate with the same frequency as the incoming photon and thus emits electromagnetic radiation with the same energy. It is thus an elastic scattering process. The Thomson-derived differential cross section for emission into a solid angle $d\Omega$ is given as

$$\frac{d_e\sigma_{Th}}{d\Omega} = \frac{r_e^2}{2}(1 + \cos^2\theta) \qquad [79]$$

and θ is the scattering angle. The cross section is independent of energy and symmetric with the same value $79.4 \times 10^{-28}\,m^2$ per (electron $\times$ steradian) at 0° and 180° and $39.7 \times 10^{-28}\,m^2$ per (electron $\times$ steradian) at 90°. The total cross section ${}_e\sigma_{Th}$ is obtained by integrating $d_e\sigma_{Th}/d\theta$ over all scattering angles θ:

$${}_e\sigma_{Th} = \int_0^{\pi} \frac{d_e\sigma_{Th}}{d\theta}\,d\theta = \frac{8\pi}{3}r_e^2 \qquad [80]$$

Experiments performed by Compton (Compton, 1923) showed, however, that the energy of the scattered photon was less than that of the primary photon. Figure 31 is taken from his original paper (Compton, 1923), showing the wavelengths of the primary photon spectrum and the wavelength spectrum for photons scattered in 90°. At that time, the radiation distribution was described using wavelengths instead of energies. In the incoherent scattering process, the photon interacts with an atomic electron, often a loosely bound electron in an outer shell, which is emitted, and the photon is scattered with a lower energy (Figure 32). Compton derived from the conservation of energy and momentum the relation between the scattered photon energy $h\nu'$ and scattering angle θ as given by eqn [81]:

$$h\nu' = \frac{h\nu}{1 + k(1 - \cos\theta)} \qquad [81]$$

where $k = h\nu/m_ec^2$ is the primary photon energy expressed in electron rest mass. Compton assumed in his derivation that the electron was free and stationary. This is not totally correct, but a good approximation in those situations, where the Compton effect dominates and many theories for cross sections and energy losses are based on these assumptions. The Compton effect is often used as a name for this interaction process, even if incoherent scattering is a more correct description. From eqn [81], it is easy to derive that for a photon scattering angle of 180°, there is a minimum in the scattered photon energy given by

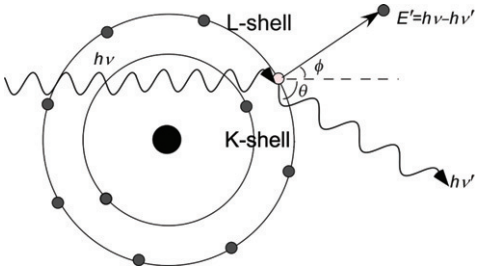

Figure 32 Schematic description of the incoherent scattering. A photon with energy $h\nu$ hits an atomic electron in an outer shell. The photon is scattered in angle θ with the energy $h\nu'$ and the electron is ejected in angle ϕ with the energy $E' = h\nu - h\nu'$.

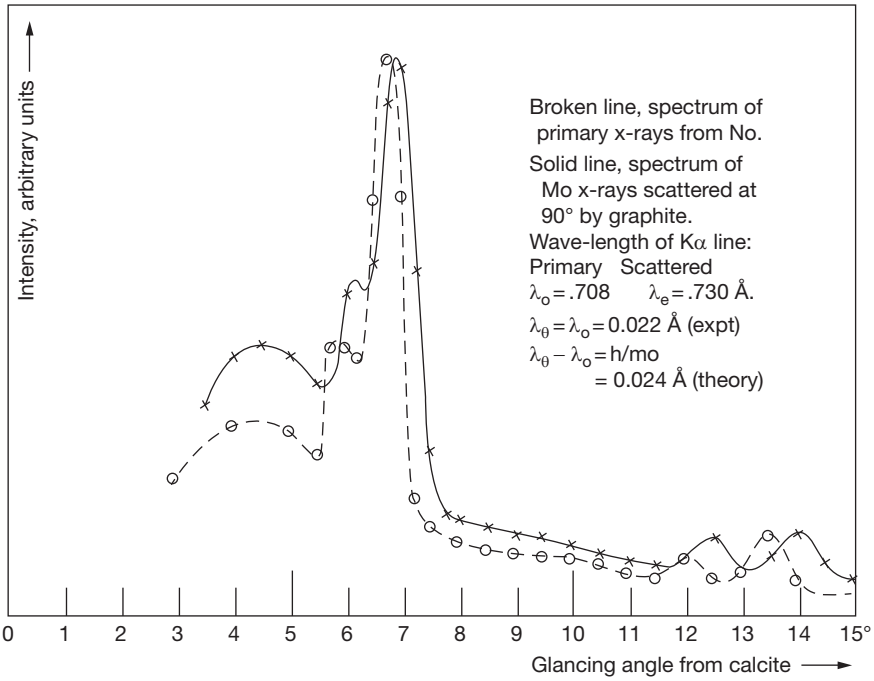

Figure 31 Spectrum of molybdenum x-rays scattered in 90° by graphite, compared with the spectrum of the primary x-rays, showing an increase in wavelength and thus a decrease in energy. Reproduced from Compton AH (1923) A quantum theory of the scattering of x-rays by light elements. *Physical Review* 21(5): 483.

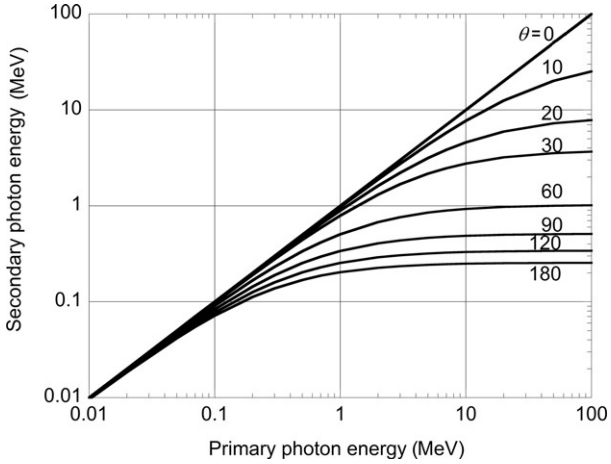

Figure 33 Scattered photon energy against the primary photon energy.

$$h\nu'_{\min} = \frac{h\nu}{1+2k} \qquad [82]$$

With increasing primary photon energy, the backscattered photon energy will reach a limit given by

$$\lim h\nu'_{\min}(h\nu \to \infty) = \frac{m_e c^2}{2} = 0.256 \text{ MeV} \qquad [83]$$

Figure 33 illustrates the relation between scattered and primary photon energies for some scattering angles. The minimum in scattered energy, $m_e c^2/2 = 0.256$ MeV at 180° and $m_e c^2 = 0.511$ MeV at 90°, when the primary photon energy goes to infinity is shown. This implies that backscattered photons in angles larger than 90° normally have energies less than 0.511 MeV. There is however a small possibility that backscattered photons scattered in several small scatterings can have a higher energy. The low-energy distribution of backscattered photons is important when calculating radiation protection shielding in situations where only large-angle scattered low-energy photons will hit the shielding wall. It is also obvious that for high photon energies, the energy transferred to the electron is high and the photon will lose a large part of its energy, while when the photon energy becomes lower, less and less fraction of the energy is transferred to the electron. This means that when a high-energy photon hits a low-atomic-number material like water, where incoherent scattering is dominating, most of its energy is lost in a couple of scattering events, but then, the photon can be scattered several times, losing little energy in each scattering event, before it may finally be absorbed by the photoelectric effect. As an illustration, consider a 10 MeV photon that is scattered in 60°. This scattered photon will get an energy of 0.93 MeV, but with further scattering events in 60°, the energy will slowly decrease and the energy will approach 0.1 MeV first after 10 scattering events. Thus, a high-energy photon can be scattered several times before being absorbed. This will influence of the transport of photons in radiotherapeutic situations. This can also be expressed as in Figure 34 where the average energies transferred to a photon and an electron, respectively, are plotted as a function of the primary photon energy. For low photon energies, most of the energy is transferred to the scattered photon, but with increasing photon energy, the energy transferred to the electron is increased.

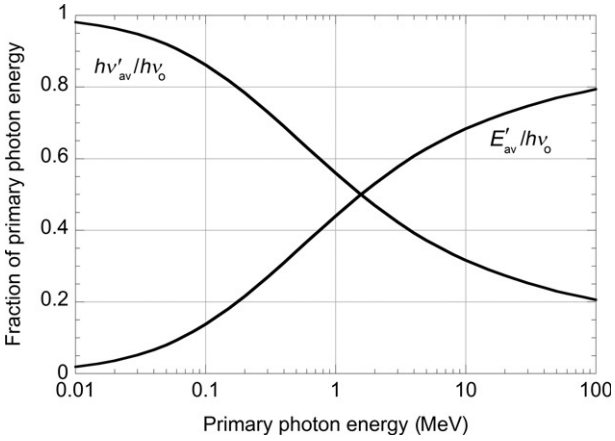

Figure 34 Variation of the scattered photon energy, $h\nu'$, and the emitted Compton electron energy, E', as a function of primary photon energy.

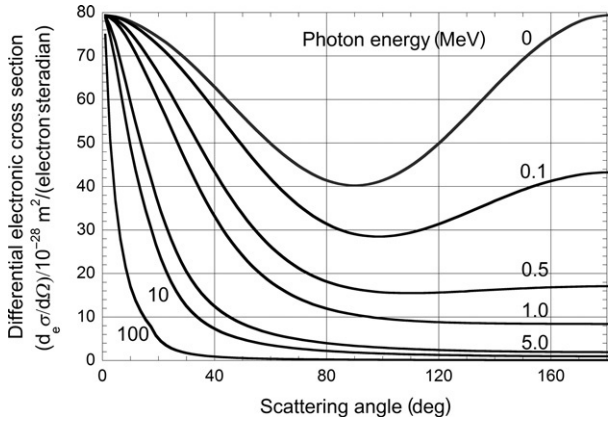

Figure 35 Differential electronic cross section for Compton effect $d_e\sigma_C^{KN}/d\Omega$ against scattering angle θ for various primary photon energies.

From eqn [81], the energy, E', of the emitted electron is easily derived.

$$E' = \frac{h\nu k(1-\cos\theta)}{1+k(1-\cos\theta)} \qquad [84]$$

The electron will get a maximum energy according to eqn [85] when it is emitted in 0° as compared to the impinging photon, which in this interaction will be scattered in 180°.

$$E'_{\max} = \frac{h\nu 2k}{1+2k} \qquad [85]$$

9.01.3.3.1 Angular distribution

The differential electronic cross section per solid angle was derived by Klein and Nishina (1929). Their derivation is based on the assumption on a collision with a free and stationary electron and is given as

$$\frac{d_e\sigma_c^{KN}(\theta)}{d\Omega} = \frac{r_e^2}{2}\frac{1}{[1+k(1-\cos\theta)]^2}\times \left[1+\cos^2\theta+\frac{k^2(1-\cos\theta)^2}{1+k(1-\cos\theta)}\right] \text{m}^2 \text{ per electron per steradian} \qquad [86]$$

This equation is reduced to the Thomson cross section when the photon energy goes to 0. Figure 35 illustrates $d_e\sigma_c^{KN}(\theta)/d\Omega$, showing that the cross section is constant for a scattering angle of 0° independent of photon energy. For very small photon energies, the cross section has the same value in 180° and half in 90°. With increasing energy, the photons are more and more forward-scattered. This implies that in diagnostic radiology with energies normally below 100 keV, the scattering angles are large and the contribution from scattered photons will deteriorate the diagnostic image and the large scattered contribution must be reduced by, for example, using grids. However, in radiotherapy with energies with several MeV, the photons are scattered in small angles and, for example, the contribution from head scatter high up in the treatment head will have less influence as they are scattered in small angles and have thus an energy close to the primary photon beam and may be treated as primary photons (Nilsson and Brahme, 1981).

For the calculation of absorbed dose and also of the contribution from emitted Compton electrons contaminating a radiotherapeutic photon beam, the angular distribution of the Compton electrons is of importance. This may be calculated from the angular distribution of the photons $d_e\sigma_c^{KN}(\theta)/d\Omega$ and considering that the relation between the electron angle and the scattered photon angle θ is given by

$$\cot \Phi = (1+k)\tan\frac{\theta}{2} \qquad [87]$$

9.01.3.3.2 Energy distribution

The energy distribution of the Compton electrons can be obtained from the Klein–Nishina cross section $d_e\sigma_C^{KN}(\theta)/d\Omega$, through the relation

$$\frac{d_e\sigma_C^{KN}}{dE} = \frac{d_e\sigma_C^{KN}}{d\Omega}\frac{d\Omega}{d\theta}\frac{d\theta}{dE} \qquad [88]$$

The energy distribution for the Compton electrons is shown in Figure 36 for photon energies between 0.5 and 10 MeV,

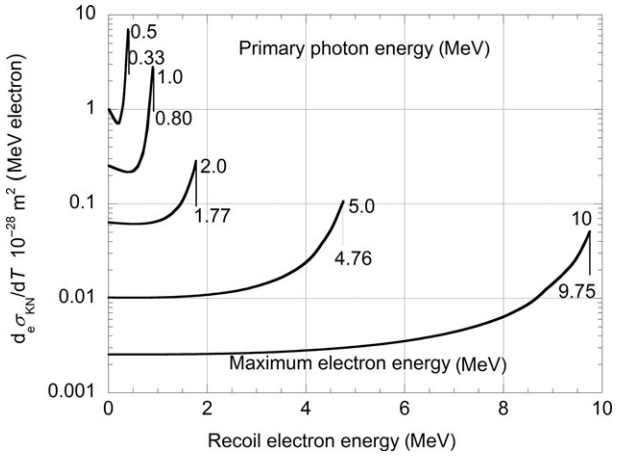

Figure 36 Differential electronic cross section per unit kinetic energy plotted against the kinetic energy of the recoil electron for primary photons energies in the range of 0.5–10 MeV.

where also the maximal Compton electron energy $E'_{max} = h\nu - h\nu'$ is indicated. This energy distribution is, for example, important for obtaining the pulse height distribution in a detector irradiated with photons, as the detected pulse height distribution will reflect the energy of the absorbed electrons. The corresponding energy distribution for the scattered photons is obtained by replacing the electron energy E by $(h\nu_0 - h\nu')$ and dE' by $d(h\nu')$.

9.01.3.3.3 Total cross section

The total electronic cross section $_e\sigma_C^{KN}$ is obtained by integrating the differential cross section per unit angle θ, $d_e\sigma_c^{KN}(\theta)/d\theta$, over all scattering angles θ. It is important to distinguish this differential cross section per scattering angle from the differential cross section per solid angle described earlier. As $d\Omega = 2\pi \sin\theta\, d\theta$, the relation between the two cross sections is given as

$$\frac{d_e\sigma_c^{KN}(\theta)}{d\theta} = \frac{d_e\sigma_c^{KN}(\theta)}{d\Omega}2\pi\sin\theta \qquad [89]$$

This cross section is illustrated in Figure 37. Integrating the differential cross section, $d_e\sigma_c^{KN}(\theta)/d\theta$, over all angles gives

$$_e\sigma_C^{KN} = \int_0^{\pi}\frac{d_e\sigma_C^{KN}}{d\theta}d\theta$$

$$= 2\pi r_e^2\left\{\frac{1+k}{k^2}\left[\frac{2(1+k)}{1+2k} - \frac{\ln(1+2k)}{k}\right] + \frac{\ln(1+2k)}{2k} - \frac{1+3k}{(1+2k)^2}\right\} \qquad [90]$$

At low photon energies, this cross section approaches the Thomson cross section:

$$\sigma_0 = \frac{8}{3}\pi r_e^2 \qquad [91]$$

For very large photon energies, the equation can be approximated by

$$_e\sigma^{KN} = \pi r_e^2\frac{2\ln(2k)+1}{2k} \qquad [92]$$

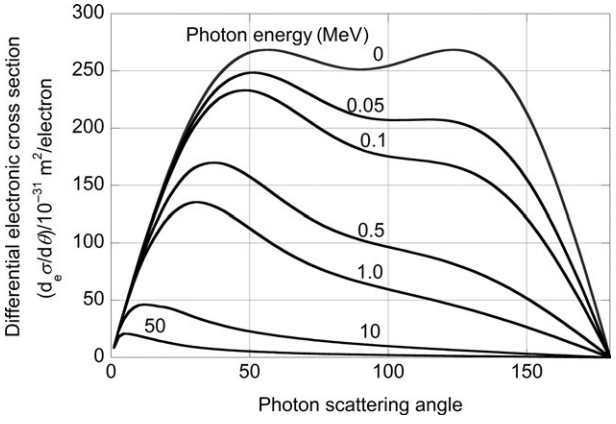

Figure 37 Differential electronic cross section for Compton effect $d_e\sigma_C^{KN}/d\theta$ against scattering angle θ for various primary photon energies.

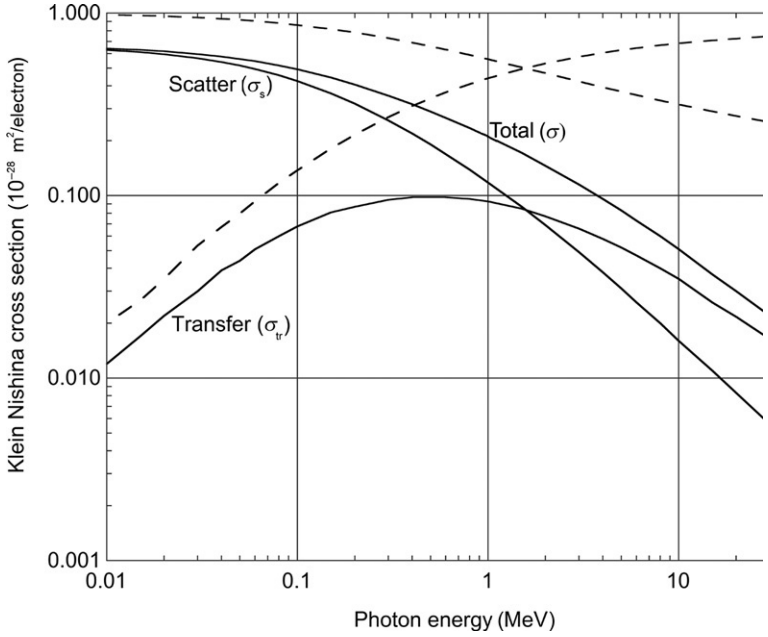

Figure 38 The scatter, transfer, and total Klein–Nishina electronic cross section for a free electron as a function of primary photon energy. The figure also includes the fractional energy transferred to the scattered photon and the Compton electron (dashed lines).

This means that the Compton cross section decreases monotonically with energy from the Thomson cross section and approaches a $1/h\nu$ dependence at high energies as illustrated in Figure 38.

The electronic Compton cross section according to Klein–Nishina is independent of the atomic number as the binding energies are neglected. The atomic cross section is then linearly proportional to the atomic number, Z. As the number of electrons per mass unit is rather constant with atomic number, the mass Compton cross section, σ_C/ρ, has a slow variation with the atomic number. When including the corrections for the binding energies (see below), there will however be larger differences at lower photon energies.

9.01.3.3.4 Mean energy transfer

The total cross section for incoherent scattering may be divided into a scattering cross section ${}_e\sigma_s$ and an absorption or a transfer cross section ${}_e\sigma_{tr}$. These cross sections give the average energies of the scattered photons and the Compton electrons through the relations

$$ {}_e\sigma_s^{KN} = {}_e\sigma_C^{KN}\frac{h\nu'}{h\nu}; \quad {}_e\sigma_{tr}^{KN} = {}_e\sigma_C^{KN}\frac{E'}{h\nu} \qquad [93] $$

Figure 38 illustrates ${}_e\sigma_s^{KN}$ and ${}_e\sigma_{tr}^{KN}$ as a function of energy together with the total ${}_e\sigma^{KN}$. In the figure are also included the fractional energies transferred to the scattered photon and the Compton electron, respectively. From the figure, it can be concluded that at low incident photon energies, a small part of the energy is transferred to the Compton electron, and with increasing energy, the fraction transferred to the Compton electron is increasing, reaching a value of 0.794 at 100 MeV incident photon energy, as discussed earlier.

9.01.3.3.5 Corrections for binding energy

The Klein–Nishina cross section is as mentioned based on the assumption that the electrons are free and at rest. However, the electrons are bound to the atomic nucleus and move in the electron orbits. This will change the cross section. If, for example, a 200 keV photon is scattered in 30°, a free electron will obtain a kinetic energy of 10 keV. If the electron is a K- or an L-electron in Pb, then this energy is lower than the binding energy and the electron cannot be emitted. The velocity of the electrons in the orbit will also affect the cross section as there will be a broadening of the scattered energy due to the Doppler effect that will depend on the velocity and the direction of the electron as compared with the incoming photon. These effects will have most influence on the cross section at low photon energies, small scattering angles, and large atom numbers of the scattering material. To include these corrections, Hubbell et al. (1975) introduced an incoherent scattering function $S(x, Z)$, where x is a transferred momentum variable and Z is the atomic number. The scattering function expresses the probability that an atom will absorb energy and be raised to an excited or ionized state when an incident photon transfers momentum to any of the atomic electrons. The incoherent scattering function $S(x, Z)$ is plotted in Figure 39 for hydrogen, carbon, aluminum, iron, and lead as a function of x. $S(x, Z)$ increases with x to reach a value equal to the atomic number at large x values. This function is multiplied with the Klein–Nishina cross section to get the differential incoherent cross section:

$$ \left(\frac{d_e\sigma_C^{BD}}{d\Omega}\right) = S(x,Z)\left(\frac{d_e\sigma_C^{KN}}{d\Omega}\right) \qquad [94] $$

Figure 40 shows the ratio of the total incoherent scattering cross section to the integrated Klein–Nishina free electron cross

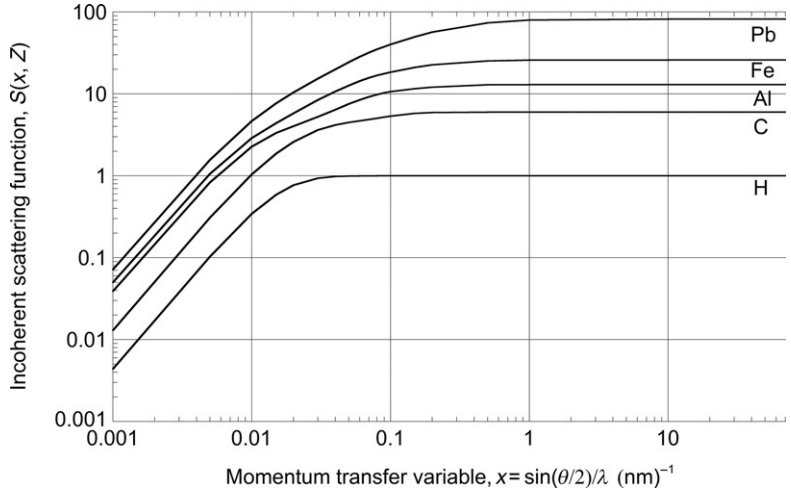

Figure 39 Incoherent scattering function $S(x, Z)$ as a function of the momentum transfer variable, x, for hydrogen, carbon, aluminum, iron, and lead.

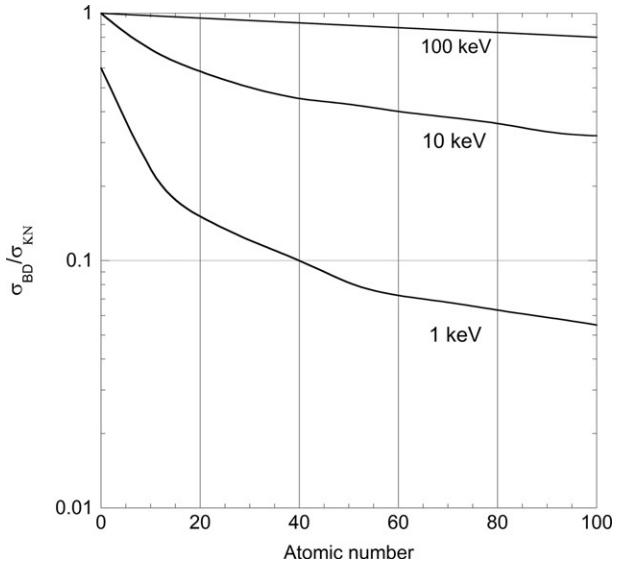

Figure 40 Comparison of the incoherent cross section ${}_e\sigma_C^{BD}$ and the Klein–Nishina cross section ${}_e\sigma_C^{KN}$ as a function of the atomic number, Z, for photon energies of 1, 10, and 100 keV. Figure adapted from Hubbell JH, Veigele WJ, Briggs EA, Brown RT Cromer D, and Howerton RJ (1975) Atomic form factors, incoherent scattering functions and photon scattering cross sections. *Journal of Physical and Chemical Reference Data* 4: 471.

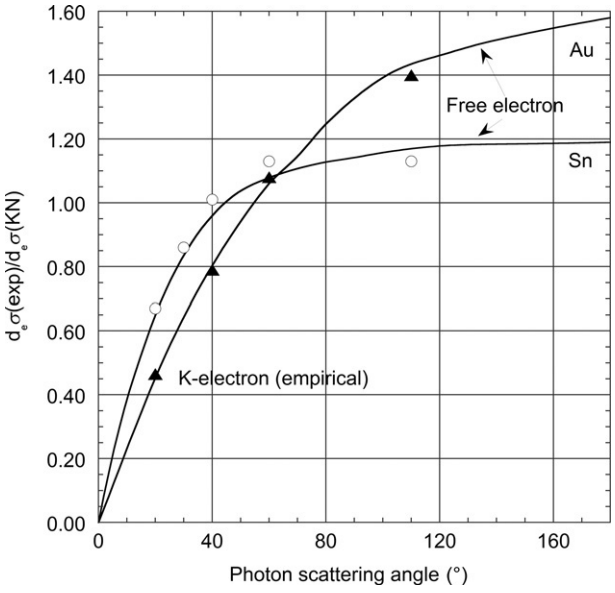

Figure 41 Ratio of observed Compton scattering from K-shell electrons to Klein–Nishina theory. Solid curves are theoretical models including the corrections for electron velocity.

section for 1, 10, and 100 keV photons as a function of the atomic number (Hubbell et al., 1975). For 100 keV photons, the ratio is close to unity except for high atomic numbers. However, for 10 keV photons, the influence of the binding energy is significant even at low atomic numbers. The binding effects will also influence the angular distribution of scattered particles. The photons will be scattered more in the forward direction. In Figure 41, the ratio between experimental incoherent scatterings from K-shell electrons to Klein–Nishina cross section data is plotted as a function of scattering angle for Au and Sn for 662 keV photons from a ^{137}Cs source. The experimental data (Motz and Missoni, 1961) are plotted as points. The solid curves are extrapolations to 180° using the theory of Jauch and Rorlich (1955) which takes electron velocity into consideration. For angles less than around 45°, the experimental data are lower than the theory, and for larger angles, the opposite holds. The corrections for the binding effects are often small in practice as they are important for energies and atomic numbers where the photoelectric effect dominates, and that is why they often are neglected in the calculations.

9.01.3.3.6 Rayleigh scattering

A photon can be scattered by the bound electrons of the atom without neither exciting nor ionizing the atom. As there in principle is no energy lost, this is close to an elastic or coherent

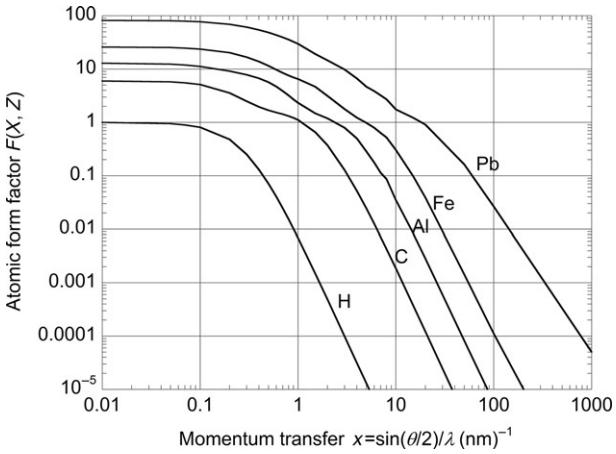

Figure 42 Atomic form factor for Rayleigh scattering plotted against the momentum transfer x for hydrogen, carbon, aluminum, iron, and lead.

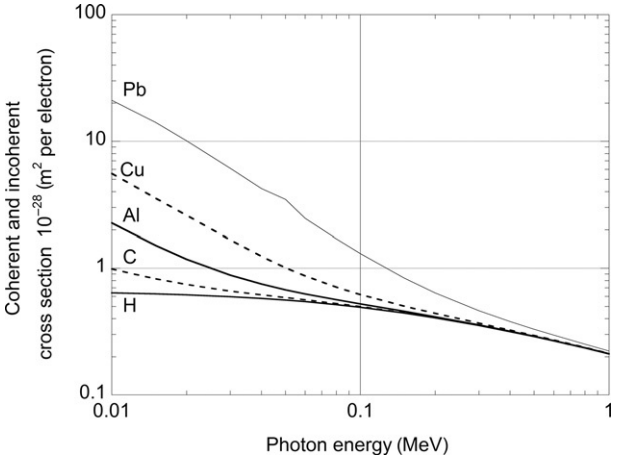

Figure 43 Electronic coherent and incoherent scattering cross section for hydrogen, carbon, aluminum, copper, and lead.

scattering and the photon continues with the same energy but is deflected. The scattering angle is often small as there are no excitation and ionization and the energy transferred to the atom must be small.

The differential Rayleigh atomic cross section $d_a\sigma_R/d\Omega$ per solid angle is obtained from the product of the Thomson cross section and an atomic form factor $F(x, Z)$ for Rayleigh scattering:

$$\frac{d_a\sigma_R}{d\Omega} = \frac{d_e\sigma_{Th}}{d\Omega}F(x,Z)^2 = \frac{r_e^2}{2}\left(1 + \cos^2\theta\right)F(x,Z)^2 \qquad [95]$$

The atomic form factor $F(x, Z)$ (Hubbell et al., 1975) is plotted in Figure 42 for the elements hydrogen, carbon, aluminum, iron, and lead as a function of $x = \sin(\theta/2)/\lambda$. The function decreases with x from a value equal to the atomic number for $x = 0$. Data show that the Rayleigh scattering is most important for low photon energies and high atomic numbers. The total scattering electronic cross section is plotted in Figure 43 where the value for hydrogen corresponds to the incoherent Klein–Nishina scattering cross section. The cross section for coherent scattering is higher than the cross section for incoherent scattering for energies smaller than around 200 keV for high atomic numbers down to less than 1 keV for low atomic numbers. The photon scattering angle is dependent on the photon energy and atomic number Z of the scatterer. An approximate expression for the angle that represents the half angle containing 75% of the Rayleigh scattered photons is given by

$$\theta_R \approx 2\arcsin\left(\frac{0.026Z^{1/3}}{k}\right) \qquad [96]$$

θ_R is plotted in Figure 44 for carbon, aluminum, iron, and lead. Included are also data for a more accurate determination of θ_R for C and Fe. The results show that the photon scattering angle increases with atomic number, Z, and decreases with energy $h\nu$. As illustrated, the approximative eqn [96] holds mainly for energies above 0.1 MeV. The importance of coherent scattering is dependent on the applicable situation. When calculating radiation protection shielding, coherent scattered photons can often be included in the primary photon beam, in particular for higher photon energies, as they have the same energy as the primary photons and are scattered in small angles and will be included in the fluence in the broad beams normally met in radiation protection calculations. However, in diagnostic radiology, they may be an important factor as they can give rise to interference effects and produce maxima in the angular distribution in crystals and their contribution to the photon fluence differential in both angle and energy has to be considered.

9.01.3.3.7 Double Compton scattering

There is also a small possibility that the scattering process by an electron on a single incoming photon will result in the emission of two photons. This process is called double Compton scattering. The probability for double Compton scattering is smaller than for single scattering, and for high energy photon energies, the ratio of double to single scattering is 1/137. The cross section for double scattering is zero for the scattering angle $\theta = 0$ resulting in an angular distribution with a maximum cross section around 20° for 10 MeV photons and around 40° for 1 MeV photons. The cross section for double scattering is included in the total cross section for incoherent scattering as tabulated by Higgins et al. (1991).

9.01.3.4 Pair Production

In pair production, a pair of particles is produced when a photon is absorbed by a target particle. In this chapter, the process, when the produced particles are an electron and a positron and the target is a nucleus or an electron, will be discussed. For further reading of pair production, the compilations by Motz et al. (1969) and Hubbell et al. (1980) are recommended. The process is illustrated in Figure 45.

The Dirac equation (Dirac, 1928) predicted particles of negative energy:

$$E_{tot}^2 = p^2c^2 + m_e^2c^4;\ E_{tot} = \pm\sqrt{p^2c^2 + m_e^2c^4} \qquad [97]$$

Dirac (1930) interpreted these negative states as particles of opposite charges to the charge of the electrons and he

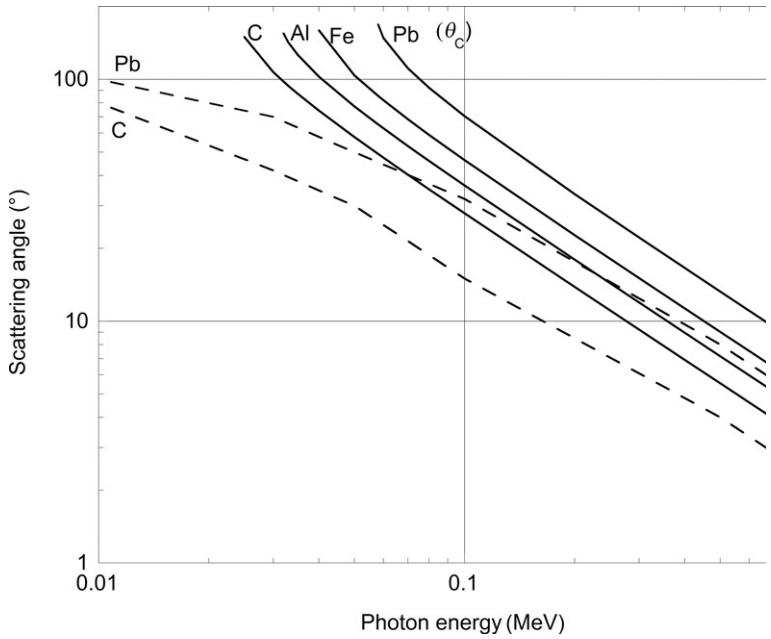

Figure 44 Scattering angles for coherent scattered photons in carbon, aluminum, iron, and lead as a function of photon energy using eqn [96]. The dashed curves are based on more accurate calculations.

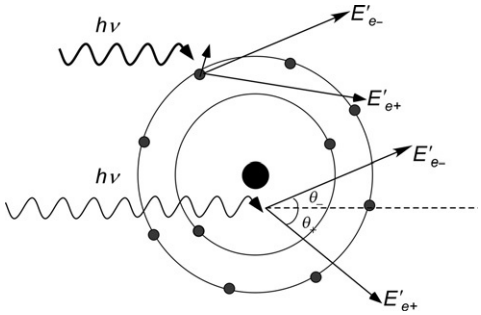

Figure 45 Schematic description of the pair production in the Coulomb field of a nucleus and an electron.

assumed that these particles were protons. However, Anderson (1932) could verify that the particles were anti-electrons or positrons.

Conservation of momentum and energy implies that this process cannot occur in free space. If in Figure 45 only the momentum component along the incident photon direction is considered, the conservation of momentum gives

$$p_\gamma = \frac{h\nu}{c} = p'_- \cos\theta_- + p'_+ \cos\theta_+ + p'_X \cos\theta_X \Rightarrow h\nu \leq p_-c' + p'_+c + p'_Xc \quad [98]$$

Using the relation

$$E_{tot} = E + m_ec^2 = \sqrt{(p')^2c^2 + m_e^2c^4} \quad [99]$$

and inserting in eqn [98], the following relation is obtained:

$$h\nu = \sqrt{(p'_-)^2c^2 + m_e^2c^4} + \sqrt{(p'_+)^2c^2 + m_e^2c^4} + E'_X \Rightarrow h\nu > p_-c' + p'_+c + E'_X \quad [100]$$

The inequalities in eqns [98] and [100] would be incompatible if there was no recoil particle and $p'_x = E'_X = 0$. This implies that there is a need for a recoil particle, which normally is an atomic nucleus but can also, with less probability, be an atomic electron. The pair production with an electron is sometimes called *triplet* production, as after the interaction, three leptons will be observed in a cloud chamber. However, one of the electrons is the atomic electron, which is emitted from the atom, and thus, this notation is not formally correct.

The kinematics will also give the threshold energies that will be obtained when the photon momentum is shared among the outgoing particles in ratio of their masses. This gives

$$h\nu_{min} = 2m_ec^2\left(1 + \frac{m_e}{m_X}\right) \quad [101]$$

When the target particle X is a nucleus, its mass m_X is much larger than the mass of the electron m_e independent of the atomic number and thus $h\nu_{min} = 2\,m_ec^2$. When the target particle is an electron, the equation gives $h\nu_{min} = 4\,m_ec^2$.

9.01.3.4.1 Energy distribution

In a pair production with the nucleus, the recoil energy to the nucleus may be neglected and the positron and the electron will get the photon energy minus the rest mass energy of the electron and positron pair.

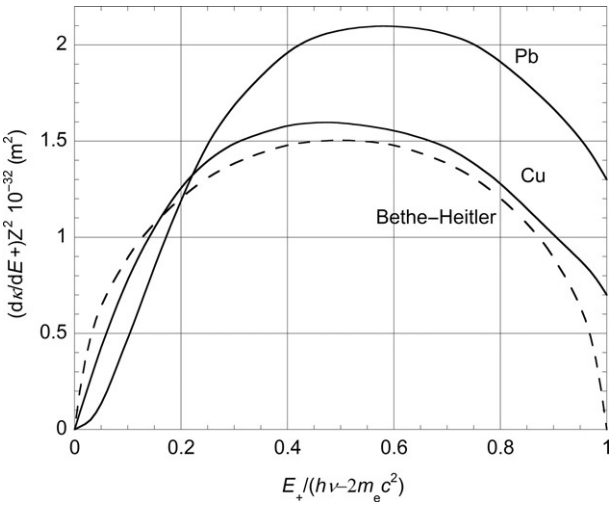

Figure 46 Dependence of the differential pair cross section $d\kappa/dE_+$ on the atomic number of the nucleus E_+ for an incident energy of 2.55 MeV. The dashed line represents the Bethe–Heitler theory.

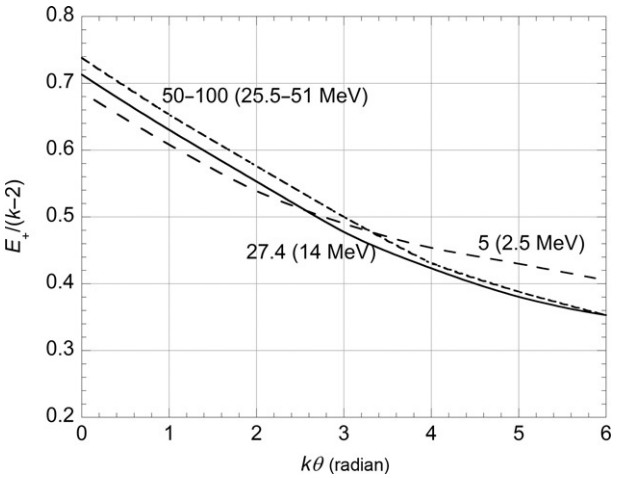

Figure 47 The variation of the average energy of the positron in pair production with the emission angle for photon energies 2.5, 14, 25.5, and 51.1 MeV. The energies are expressed in electron rest mass energy.

$$E_{e-} + E_{e+} = h\nu - 2m_ec^2 \qquad [102]$$

The energy distribution for the positron can approximately be given as

$$\frac{d\kappa}{dE_+'} = Z^2 r_e^2 \alpha g\left(h\nu, E_+', Z\right) \qquad [103]$$

The function $g(h\nu, E_+', Z)$ increases with increasing $h\nu$ and decreases slightly with increasing Z. The electron and the positron will share the energy, and in the first approximation, the probability for a kinetic energy between 0 and $h\nu - 2\,m_ec^2$ is nearly constant. However, at low photon energies, the positive charge of the nucleus will have an effect on the energy distribution resulting in a slightly higher energy of the positron (Øverbø et al., 1968). This effect is illustrated in Figure 46 for copper and lead irradiated with 2.55 MeV photons. The symmetrical distribution as a result of eqn [103] based on the Bethe–Heitler–Born approximation is also included. The energy distribution will also slightly depend on the scattering angle. Figure 47 shows the mean energy as a function of the scattering angle and photon energy for 2.5, 14, 25.5, and 51 MeV (Nilsson and Brahme, 1983). In the figure, the energies are expressed in electron rest mass energy. The mean energy decreases slowly with the parameter $E_+/(k-2)$ from 0.7 at small angles to 0.4 at large emission angles.

9.01.3.4.2 Angular distribution

The angular distribution of the electrons and positrons is depending on the energy of the incoming photon, and with higher energies, the more forward-emitted are the particles. An expression for the cross section of the angle of divergence, Δ, is in the high-energy region given by Borsellino (1953)

$$d\sigma = 16\alpha(Zr_e)^2 f(1-f)F\frac{x\,dx}{(1+x^2)^2} \qquad [104]$$

where $f = E_+/h\nu$, $x = \Delta/\Delta_0$ and F is a function of the incident photon energy and momentum transferred to the positron. If the positron and the electron shares the energy equally,

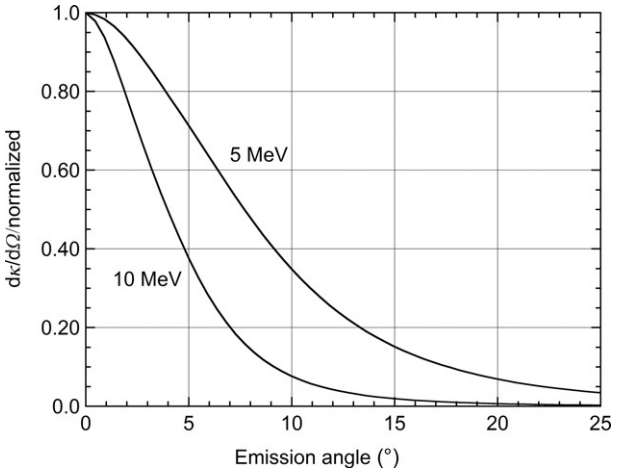

Figure 48 Approximative angular distribution, $d\kappa/d\Omega$, of the emitted positrons in a pair production process assuming that the Bethe approximation holds and the transferred energy are divided equally between the positron and the electron.

$\Delta_0 = 4\,m_ec^2/h\nu$. In the Bethe approximation, F is a constant. Figure 48 shows a normalized angular distribution, $d\sigma/d\Omega$, for the positron for 5 and 10 MeV photons calculated using the Bethe approximation. The emission angles decrease with the energy approximately as $1/h\nu$.

9.01.3.4.3 Total cross section

The total atomic cross section for pair production ${}_a\kappa_n$ is obtained by starting with the Born approximation for an unscreened point nucleus (Bethe and Heitler, 1934). This cross section is often called ${}_a\kappa_n^{BH}$. To this cross section are then added Coulomb correction as the nucleus is not a point charge, screening correction from the electron shells, and radiative correction due to the accelerating charge.

Racah (1936) proposed an expression for the unscreened point nucleus Born approximation. Equation [105] is based on his expression

$$ {}_a\kappa_n^{BH} = \alpha Z^2 r_e^2 \left\{ \frac{28}{9} \ln 2k - \frac{218}{27} + \left(\frac{2}{k}\right)^2 \right\} f(k) \qquad [105] $$

This equation indicates that there is a Z^2 dependence and that the cross section slowly increases with energy k.

The Coulomb correction is small for low atomic numbers and less than 1% for carbon. For high atomic numbers as, for example, lead, the correction is however large, in particular at low photon energies, and has to be included. This correction is based on both theories and empirical methods. For high energies, interaction may take place at large distances from the nucleus and shell electrons can then screen the effect of the atomic nucleus. This will reduce the cross section and the cross section will approach a saturation value at very high photon energies. The radiative correction is small and approaches 1% for energies above 50 MeV. An expression for the high-energy cross section with a complete screening is given in eqn [106].

$$ {}_a\kappa_n^{screened} = \alpha Z^2 r_e^2 \left\{ \frac{28}{9} \ln 2k - f(Z) \right\} \qquad [106] $$

The atomic cross section for pair production is plotted in Figure 49 for aluminum and lead divided with Z^2 for pair production with the nucleus and with Z for pair production with the electron. The figure illustrates the Z^2 dependence for the pair production with the nucleus for energies below some MeV and the effect of screening at higher energies, which is more important for higher atomic numbers.

9.01.3.4.4 Pair production in the field of an electron or triplet production

The theoretical treatment of the pair production in the field of an electron should include (Hubbell et al., 1980) atomic binding of the target electron, screening by other atomic electrons and by the field of the nucleus, retardation which occurs when the atomic electron recoil velocity is not negligible in comparison with the velocity of light, the γ–e interaction of the incident photon with the atomic electron, exchange terms resulting from the difficulty to distinguish between the two electrons, and radiative corrections. No treatment has included all of these six effects, which means that the numerical values are based on a combination of different theoretical treatments. Borsselino (in Roy and Reed, 1968) has derived an expression for an unscreened atom including only corrections for retardation.

$$ {}_a\kappa_e^{BH} = \alpha Z r_e^2 \left\{ \frac{28}{9} \ln 2k - \frac{218}{27} - f(k) \right\} \qquad [107] $$

This equation is similar to the cross section ${}_a\kappa_n^{BH}$, for pair production in the field of a nucleus, but proportional to Z instead of Z^2. This indicates that the cross section for pair production in the electron field is less than the one in the field of a nucleus and the ratio may be expressed as

$$ \frac{{}_a\kappa_e}{{}_a\kappa_n} = \frac{1}{CZ} \qquad [108] $$

where C is nearly independent on the atomic number but depends on the photon energy and is about three at low photon energies and close to one for high energies. The cross section divided with Z is plotted in Figure 49. The figure illustrates in a similar way as for ${}_a\sigma_n$ the Z dependence for lower photon energies and the screening effect at higher energies.

The energy distribution in a pair production with an electron is given by the relation

$$ h\nu = 2m_e c^2 + E_{e-} + E_{e+} + E_{orb.el} \qquad [109] $$

The available energy is distributed to the three particles within the energy limits given by Perrin (1933)

$$ E = \frac{k^2 - 2k - 2 \pm k\sqrt{k(k-4)}}{2k+1} m_e c^2 \qquad [110] $$

This will, for example, for a 20 MeV photon, result in that the kinetic energies of the three particles will lie between the limits of 0.68 keV and 18.7 MeV. The recoil orbital electron will often get very little kinetic energy, so most of the energy is divided between the produced electron–positron pair.

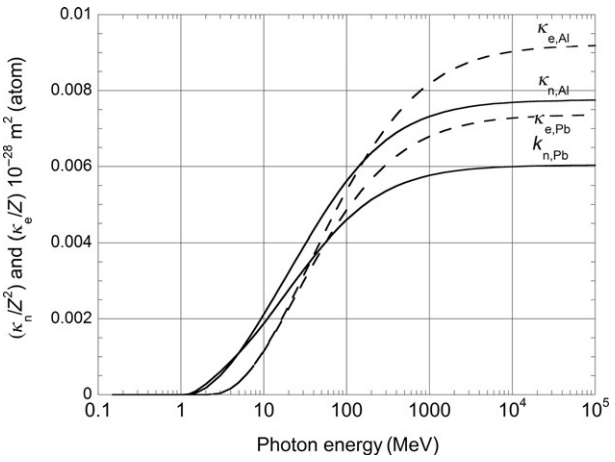

Figure 49 Atomic cross section for pair production with the nucleus (solid curves) and electron (dashed curves) divided by Z^2 and Z, respectively. Data from Berger et al. (2005a).

9.01.3.4.5 Positron annihilation

A corollary reaction to pair production is annihilation. In this process, the positron annihilates with an electron and the energy is emitted as electromagnetic radiation. One, two, or three photons are emitted in the process.

One quantum annihilation. If the electron is strongly bound to the nucleus, only K-electrons are included in the theories, it is possible with emission of a single photon, and the excess recoil momentum is being absorbed by the atomic nucleus. The cross section is given by Heitler (1954) as

$$ \sigma_1 = \frac{4\pi}{Z} (\alpha Z)^4 (Z r_e)^2 f(E_+) \qquad [111] $$

This cross section has a maximum for a positron energy around 0.25 MeV and decreases fast with decreasing energy. Generally, the cross section is small compared with two-quanta

annihilation, but for high atomic material, σ_1/σ_2 may be significant. If, for example, $Z=82$ and the positron energy is 5 MeV, σ_1/σ_2 is ≈ 0.2. One quantum annihilation is forbidden with a free electron since conservation of energy and momentum is then impossible.

Two-quanta annihilation. Two-quanta annihilation is the most common annihilation process. In this case, the electron is assumed to be free. Then, the momentum conservation demands that more than one photon is emitted. Dirac has derived an expression for two-quanta annihilation. The cross section increases with decreasing energy. For low energies, that is, when $v_+ \ll c$, the cross section can be approximated as

$$\sigma_2 = \pi r_e^2 \frac{c}{v_+} \qquad [112]$$

In the limit when the positron energy and thus the velocity are very small, the cross section would go to infinity. In this situation, the number of annihilation processes per unit time, P, is limited by the reciprocal of the free positron lifetime in a medium of free electrons:

$$P = \tau^{-1} = \pi r_e^2 \rho \qquad [113]$$

where ρ is the free electron density in the medium. For very slow positrons in lead, τ is of the order of 10^{-10} s.

In the most common situation, the positrons are thermalized before they are annihilated, usually then with valence electrons. In this situation with assumed negligible momentum input, the two photons will have the energy 0.511 MeV and they will be emitted at directions separated by 180°. In fact the momentum before annihilation is not completely negligible. This will imply that the photons depart at relative angles distributed around 180° with an angular width of about 1°. The photon energy spread is often about 10 eV if the positron energy is low.

Two-quanta annihilation for thermalized positrons is valuable in diagnostic nuclear medicine, as with a positron camera, it is possible to determine the position of the annihilation point. As the positrons emitted from radionuclides, like ^{11}C, ^{15}O, and ^{18}F, that often are used in these types of investigations have low kinetic energies, the annihilation point is close to the positron decaying radionuclide. It is thus possible to obtain a distribution of the radioactivity in the body. Nuclides like carbon and oxygen are present in the body, and positron camera investigations are of major diagnostic value.

There is, however, a probability that relativistic positrons can annihilate in flight prior to thermalization. In this case, one photon is emitted in the forward direction with nearly all energy, and the other low-energy photon is observed at a large angle to the direction of the incident positron. The probability for annihilation in flight is higher for high-energy positrons but has a slow variation with atomic number. For 5 MeV positrons, the probability for annihilation in flight is 10% for Be and 13% for U decreasing to 3% and 5% for a 1 MeV positron, respectively. One application of annihilation in flight is that it is possible to produce nearly monoenergetic photons that are very useful in studies of photonuclear reactions. Information on annihilation in flight is also of importance when calculating mass energy absorption coefficients.

Three-quanta annihilation. This is an unlikely process and is forbidden for a free electron–positron pair, since conservation of energy and momentum between initial and final states is then impossible. The ratio of the three quanta to the two quanta cross section is given as

$$\frac{\sigma_3}{\sigma_2} = 1.159\frac{\alpha}{\pi} = 2.69 \times 10^{-3} \qquad [114]$$

9.01.3.5 Photonuclear Reactions

Photons may react with the nucleus with the result of emission of mainly a single neutron, but also protons, γ-rays, and more than one neutron can be emitted. The threshold energy needed for this process is for many atomic numbers in the region of 6–16 MeV except for some isotopes with low atomic number as deuterium and beryllium with thresholds of 2.2 and 1.67 MeV, respectively. Some threshold values for (γ, n) and (γ, p) reactions are listed in Table 2. The threshold values for (γ, p) are lower than those for (γ, n) due to the Coulomb repulsion in the nucleus, but the cross section is lower because of the large Coulomb barrier against proton emission. Above the threshold, the cross section can be described by a 'giant resonance' giving a maximum value around 24 MeV for low-atomic-number nuclei and 12 MeV in high atomic numbers (see Table 2). The distribution does not have only one maximum point but some substructures, which often can be described by two main peaks. The FWHM of the resonance varies between 3 and 9 MeV depending on the properties of the nuclei.

The maximum value of the (γ, n) cross section leading to the emission of a neutron is of the order of 10×10^{-28} m^2 in low-atomic-number materials and increases to around 400×10^{-28} m^2 for high atomic numbers. With higher photon energies, $\geq$20–30 MeV, it is possible to obtain also emission of more than one particle, and reactions like (γ, 2n) and (γ, pn) appear.

Table 2 Photonuclear parameters for some nuclides.

Absorber	*Threshold for (γ, n) MeV*	*Threshold for (γ, p) MeV*	*Resonance peak energy (MeV)*	*Percent of total cross section for (γ, n)*
^{9}Be	1.67	–	–	–
^{12}C	18.7	15.9	23.0	5.9
^{16}O	15.7	12.1	–	–
^{27}Al	13.1	8.3	21.5	3.9
^{63}Cu	10.8	6.1	17.0	2.0
^{206}Pb	8.1	7.3	13.6	2.7

Data from Podgorsak EB (2009) *Radiation Physics for Medical Physicists*. Springer: Berlin; Attix FH (1986) *Introduction to Radiological Physics and Radiation Dosimetry*. Wiley: New York.

In low atomic numbers, the cross section for photonuclear reactions is always lower than some percent of the total cross section, and in most tabulations of the photon cross sections, this cross section is not included, partly also due to the uncertainties in the numerical value of the cross section.

The (γ, n) reactions will produce neutrons, and in radiotherapy with high-energy photon beams, there will be a neutron contribution to the absorbed dose in the patient. This contribution is low and can normally be neglected. However, it is important to consider these neutrons when constructing the shielding in radiotherapy treatment rooms. Another aspect is that as a result of these (γ, n) and (γ, p) reactions, the stable target nucleus can be radioactive after the interaction. For example, after a (γ, n) reaction, ^{12}C will be transformed to ^{11}C, ^{14}N to ^{13}N, and ^{16}O to ^{15}O with half lives of 20.4 min, 10.0 min, and 122 s, respectively. This will imply a radiation protection problem in radiation therapy with high photon energies, as the air in the room will be radioactive and there is a need for a forced ventilation. Another aspect is that the patient will be radioactive and the activity distribution can be used for checking the given dose distribution in the patient by measuring the patient with a positron camera directly after treatment (Janek et al., 2006; Janek Straat et al., 2013).

9.01.3.6 Mass Attenuation and Absorption Coefficients

As mentioned, the total macroscopic attenuation cross section is the sum of all cross sections for the different interaction processes (photoelectric effect, Rayleigh scattering, incoherent scattering, pair production in the field of the nucleus, and the electron). The photonuclear cross section is not normally included. There are different ways of expressing the cross sections, as an electronic, an atomic, a linear, or a mass cross section, which is the most common way to tabulate the cross sections. In this paragraph, three different coefficients will be discussed, the mass attenuation coefficient (μ/ρ), the mass energy transfer coefficient (μ_{tr}/ρ), and the mass energy absorption coefficient (μ_{en}/ρ).

9.01.3.6.1 Mass attenuation coefficient

The relative contribution from the different interaction processes varies with photon energy and atomic number. In Figure 50, the relative fractions of the cross sections are plotted for carbon and lead. The absolute values are plotted in Figure 51 for the same materials. All data are taken from the NIST data table (http://nist.gov/pml/data), where attenuation coefficients and cross sections are tabulated. It is also possible to calculate new cross sections for materials not included by using the program XCOM (Berger and Hubbell, 1990). From Figure 50 and Figure 51, some conclusions of the variation of μ/ρ with atomic number and energy can be made. For low-atomic-number materials, typical for tissue, incoherent scattering dominates over a large energy range, from around 10 keV to more than 10 MeV. Thus, for energies typical in radiotherapy, incoherent scatter will have an important influence of the transport of photons in soft tissue. In high-atomic-number materials as lead, on the other hand, photoelectric effect is dominant up to some hundred keV and pair production will start to dominate at energies around 5 MeV. This is one of the reasons that high atomic numbers often are good absorbers. The high dependence of the atomic number for the photoelectric effect is also valuable in diagnostic radiology, as even tissues with a small difference in atomic number will be visible. For energies around 1 MeV, μ/ρ has similar value in carbon and lead and thus the narrow-beam attenuation will be close in the two materials, but due to the different contribution from the individual cross sections, the transport of photons through the same thickness expressed in kg m^{-2} will differ significantly.

The cross sections are based both on partly approximative calculations and also on partly experimental data, indicating uncertainties in the tabulated values. Trubey et al. (1989) estimated the uncertainties in the available data. Their conclusions of the maximum estimated uncertainties in the total attenuation coefficient are summarized in Table 3. For energies normally used in diagnostic radiology and radiotherapy, 50 keV to 20 MeV, the uncertainties are around 2%, but for very low energies, below 1 keV, Table 3 indicates very large uncertainties and a dependence of the phase of the material.

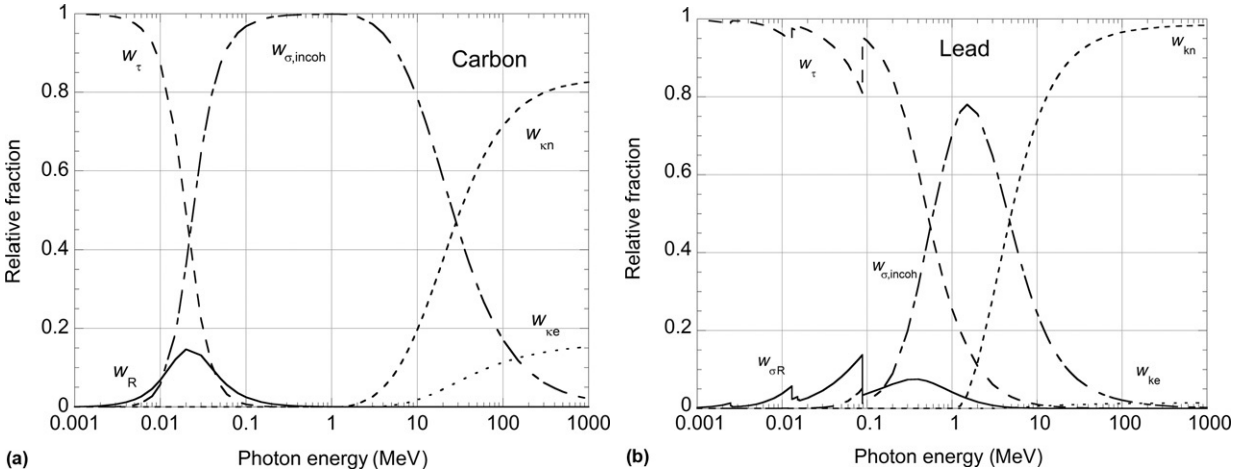

Figure 50 Relative contributions of various photon interactions as a function of photon energy for (a) carbon and (b) lead.

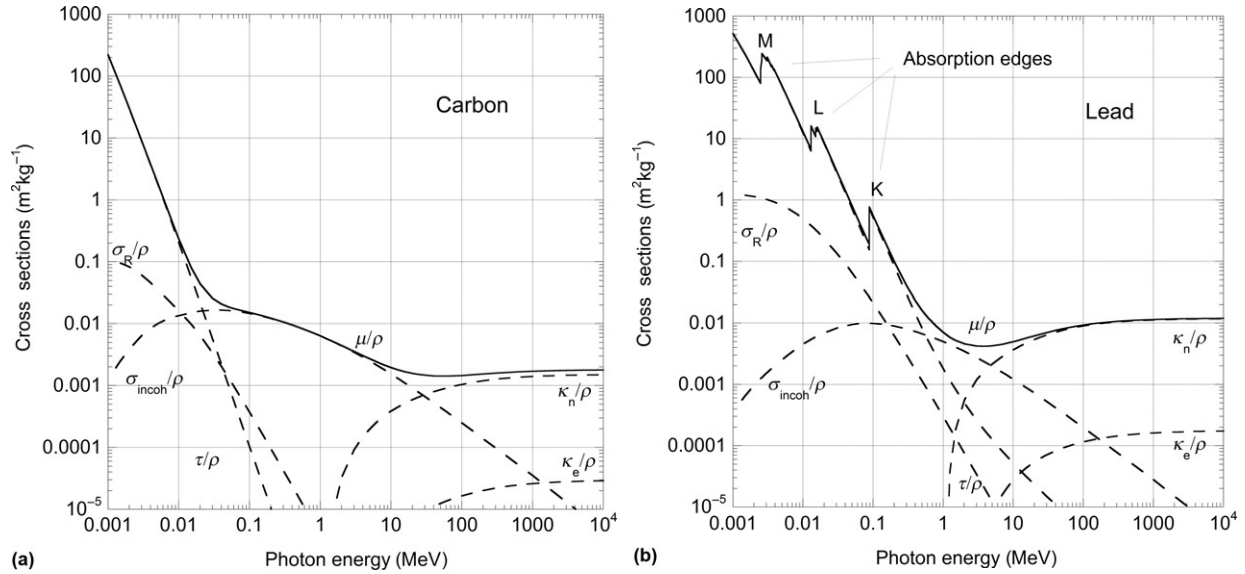

Figure 51 Mass attenuation coefficient μ/ρ as a function of photon energy for (a) carbon and (b) lead. The separate contributions from photoelectric effect, τ/ρ, Rayleigh scattering, σ_R/ρ, incoherent scattering, σ_{incoh}/ρ, and pair production in the field of a nucleus, κ_n/ρ, or an electron, κ_e/ρ, are also included.

Table 3 Maximal uncertainties in the mass attenuation coefficient

Energy range	*Solid (%)*	*Gas (%)*
10–100 eV	1000	20
0.1–0.5 keV	100–200	10–20
0.5–1.0 keV	10–20	5
1.0–5.0 keV	5	5
5.0–100 keV	2	2
0.1–10.0 MeV	1–2	1–2
10 MeV–100.0 GeV	2–5	2–5

In diagnostic radiology, the atomic number dependence of mass attenuation coefficients is used to differentiate between tissues. In some situations as mammography or angiography, the contrast may however be too small. Then, x-ray phase-contrast imaging techniques could be useful. The use of phase contrast will increase the attenuation contrast as shown in Figure 52 where δ/β is the attenuation contrast ratio plotted for breast, water, and bone together with the attenuation coefficients for bone and water. For energies 20–80 keV, the phase contrast is large and will result in images of much higher contrast than in traditional radiology (Zhou and Brahme 2008).

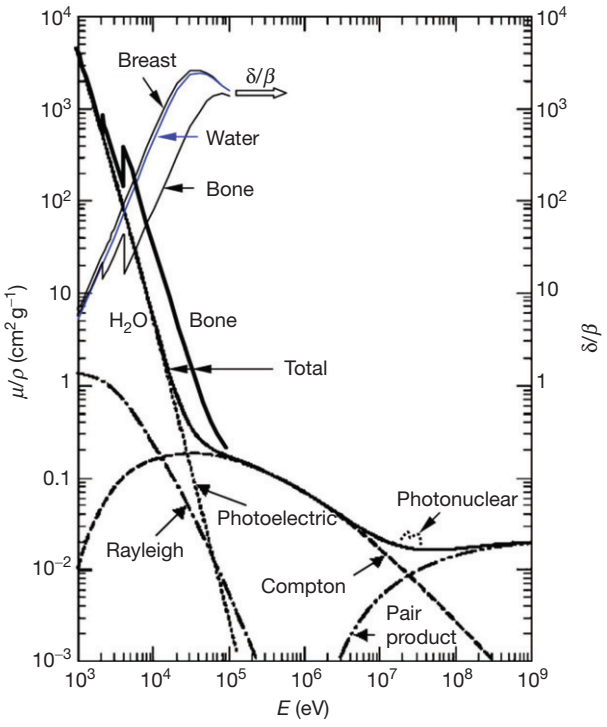

Figure 52 Dependence on the phase to attenuation contrast ratio δ/ρ for breast tissue, water, and cortical bone and dependence on the mass attenuation coefficient of water and cortical bone (Zhou and Brahme (2008).

9.01.3.6.2 Mass energy transfer coefficient

In dosimetry, it is often of interest to determine the energy transferred to the electrons in the photon interaction processes. This is obtained by multiplying the interaction cross sections with the relative energy transferred in each interaction. To handle this, the mass energy transfer coefficient has been defined (ICRU, 2011):

$$\frac{\mu_{tr}}{\rho} = \frac{1}{\rho\, dl}\frac{dR_{tr}}{R} \qquad [115]$$

where dR_{tr} is the mean energy that is transferred to kinetic energy of charged particles by interactions of the photons of incident radiant energy R in traversing a distance dl in the material with density ρ. (μ_{tr}/ρ) is obtained by calculating the transferred energy in the different interaction processes as described briefly in the following paragraphs.

Photoelectric effect. In photoelectric effect, not only photoelectrons but also Auger electrons of different energies

are emitted. It has been found easier to calculate the energy transferred to the characteristic x-rays and subtract their energy from the energy of the incoming photon instead of directly calculate the energy to the electrons. Thus,

$$\frac{\tau_{tr}}{\rho} = \frac{\tau}{\rho}\left[1 - \frac{p_K \omega_K h\nu_K}{h\nu} - \frac{(1-p_K)p_L\omega_L h\nu_L}{h\nu} + \cdots\right] \qquad [116]$$

where $p_{K,L}$ is the fraction of photoelectric interactions in the K- and the L-shell, respectively, $\omega_{K,L}$ is the fluorescence yield, $h\nu_{K,L}$ is the energy of the characteristic x-rays, and $h\nu$ is the incoming photon energy. In this equation, the contribution from outer shells is neglected but can be included as well, even if this contribution normally is small.

Incoherent scattering. In coherent scattering, the electrons will get a distribution of energies given by the Klein–Nishina cross section as discussed earlier. Corrections for the binding effects are included using the incoherent scattering function $S(q, Z)$. Then, the mass energy transfer for incoherent scattering can be expressed as (Higgins et al., 1991)

$$\frac{\sigma_{tr}}{\rho} = (1 + \Delta_{KN})\int_0^{\pi} (d\sigma_{KN}/d\Omega) S(q, Z)\frac{E}{h\nu} d\theta \qquad [117]$$

Pair production. The fraction of photon energy transferred to the electron positron pair is given by the photon energy subtracted with the rest mass energy of the produced particles. Thus,

$$\frac{\kappa_{tr}}{\rho} = \frac{\kappa}{\rho}\frac{h\nu - 2m_e c^2}{h\nu} \qquad [118]$$

(μ_{tr}/ρ) is then obtained by adding the different components:

$$\frac{\mu_{tr}}{\rho} = \frac{\tau_{tr}}{\rho} + \frac{\sigma_{incoh,\,tr}}{\rho} + \frac{\kappa_{tr}}{\rho} \qquad [119]$$

9.01.3.6.3 Mass energy absorption coefficient

Part of the energy transferred to the electrons will be lost as electromagnetic radiation when the electrons are absorbed in matter. It is common in dosimetry to assume that this energy is not included in the absorbed dose at the spot where the interaction occurs, as the photons can travel far before they are absorbed. The 'locally' absorbed energy can be determined using the mass energy absorption coefficient. The mass energy absorption coefficient can be obtained from the mass energy transfer coefficient through the relation

$$\mu_{en}/\rho = (\mu_{tr}/\rho)\,(1 - g) \qquad [120]$$

where g is the kinetic energy lost by the electron in radiative processes (bremsstrahlung, in-flight annihilation, and characteristic x-rays) when the charged particles slow to rest in the material.

In many situations, in particular at low photon energies below around 500 keV, a so-called charged particle equilibrium (CPE) is assumed to exist. In this situation, the absorbed dose to the medium can be obtained from the relation

$$D = \int \Psi_{h\nu}(\mu_{en}/\rho)\, d(h\nu) \qquad [121]$$

where $\Psi_{h\nu}$ is the differential energy photon fluence and μ_{en}/ρ is the mass energy absorption coefficient.

In Figure 53, the mass attenuation coefficient, mass energy transfer coefficient and the mass absorption coefficient are plotted for carbon and lead as a function of the photon energy. The different absorption coefficients agree quite well at low photon energies where the photoelectric effect dominates. However, in the energy region with a dominating incoherent scattering, a large fraction of the photon energy will be transferred to the electron, with a large difference between the attenuation and energy absorption coefficient, which is obvious, in particular for carbon. At high photon energies, the pair production will dominate and a small part of the energy is transferred to the electrons. At these high energies, there will also be a difference between the mass energy transfer and mass energy absorption coefficients, as in particular, bremsstrahlung will become important. As bremsstrahlung production is proportional to the square of the atomic number, this difference is more evident for lead than for carbon.

In a situation when there is no CPE, it is not possible to use eqn [121], as then, the energy contribution from electrons entering a volume, for example, a detector, will not be compensated

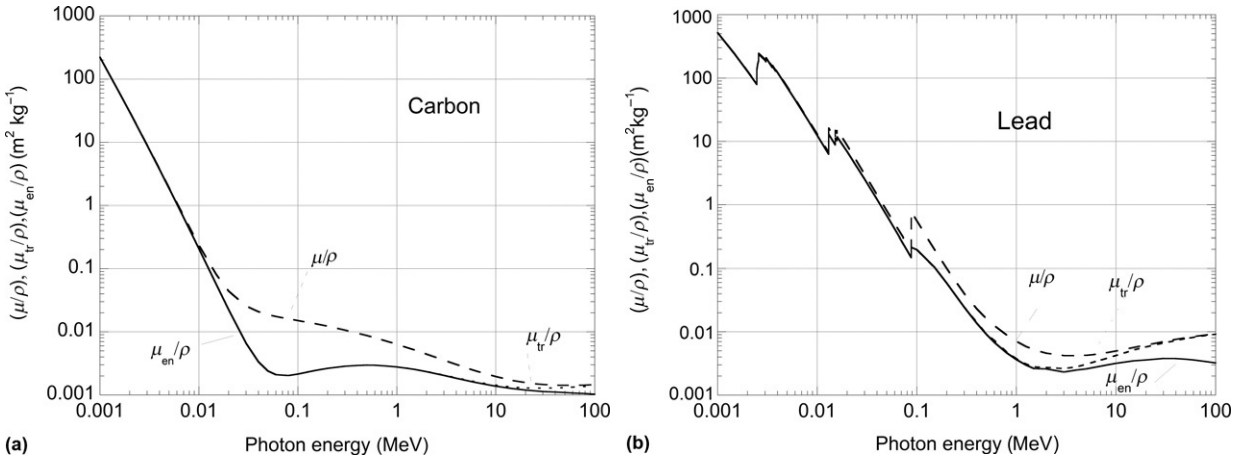

Figure 53 Mass attenuation coefficient, $\mu(\rho)$, mass energy transfer coefficient, μ_{tr}/ρ, and the mass energy absorption coefficient, μ_{en}/ρ, as a function of photon energy for carbon and lead.

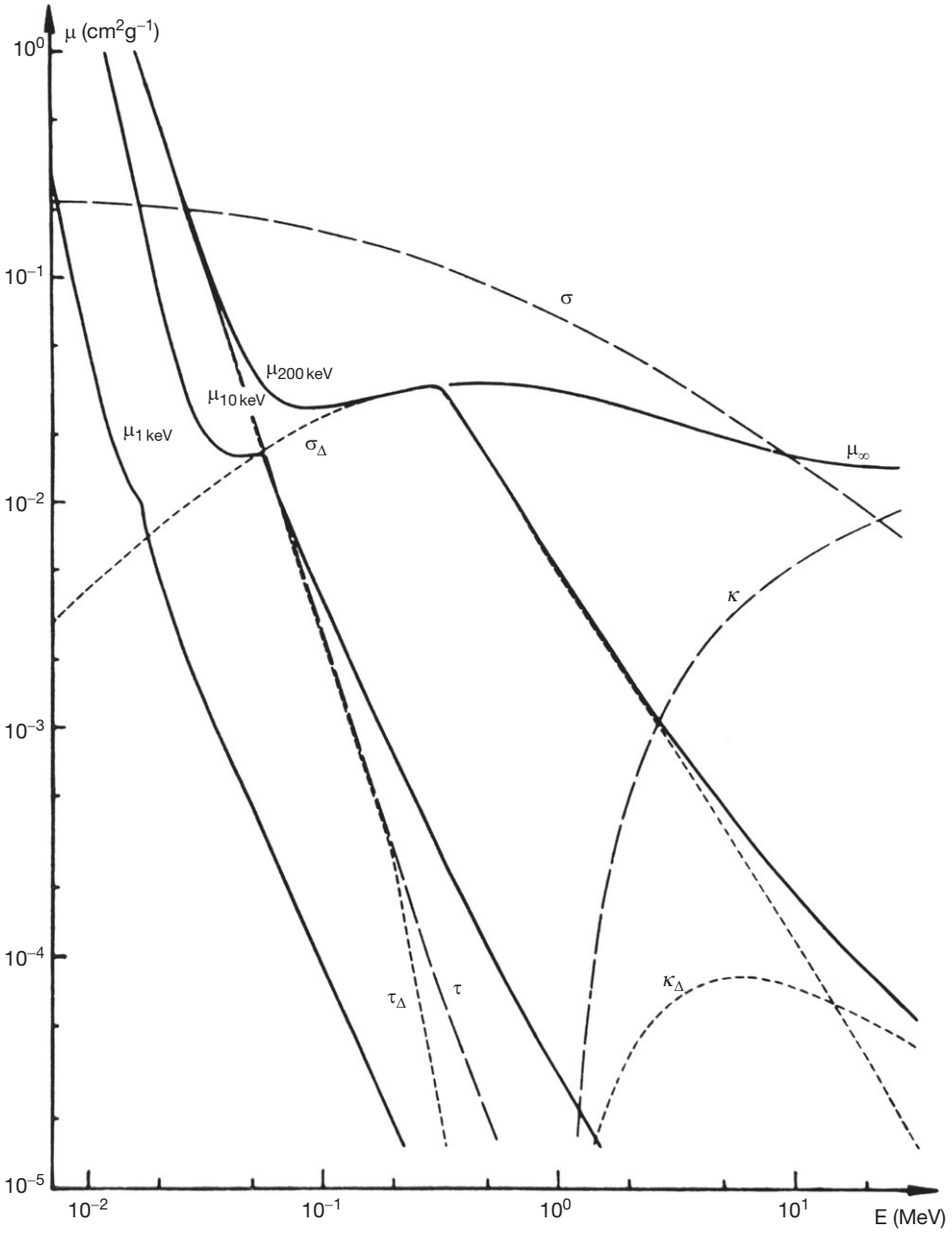

Figure 54 Restricted mass energy absorption coefficients for water as calculated for energy restrictions of 1, 10, and, 200 keV. At 200 keV, the elementary contributions from photoelectric, incoherent scattering, and pair production processes are indicated. (Brahme, 1978).

by the electron energy leaving the volume and the use of the mass energy absorption coefficient, which includes all energy deposited by the photon produced electrons, is not correct. For a situation without CPE, Brahme (1978) had proposed the use of a restricted mass energy absorption coefficient, μ_{Δ}/ρ. This coefficient shall include only the fraction of the secondary electron energy that is absorbed within a small volume around the primary photon track. The size of the region R_{Δ} is chosen to correspond to the range of the secondary electrons of some restriction energy Δ. The energy restriction, Δ, is related to the energy restriction of the mass stopping power to be used in the same region. The restricted mass energy coefficient can be used in cavity theories to calculate the fraction of the absorbed dose to a volume that is due to photon interactions in the cavity. The ratio of absorbed doses between the dose in the detector, D_{d}, and the medium, D_{m}, can then be expressed as

$$\frac{D_{\mathrm{d}}}{D_{\mathrm{m}}} = \left(\frac{S_{\Delta}}{\rho}\right)_{\mathrm{m}}^{\mathrm{d}} + \left(\frac{\mu_{\Delta}}{\mu_{\mathrm{en}}}\right)_{\mathrm{d}} \left(\frac{\mu_{\mathrm{en}}}{\rho}\right)_{\mathrm{m}}^{\mathrm{d}} \qquad [122]$$

Equation [122] is partly similar to the general cavity theory for intermediate cavities as proposed by Burlin (1966). However, in eqn [122], the weighting factor for the contribution of the electrons produced in the detector is obtained directly from the restricted mass energy absorption coefficient, while in the Burlin expression, the contribution is obtained indirectly from the

absorption of the electron slowing down spectrum. Equation [122] was applied to an ionization chamber with similar results as for the Burlin cavity theory, indicating that this concept could be of value for intermediate cavities. Brahme (1978) calculated numerical values of μ_Δ for Δ-values between 1 and 100 keV and the result is shown in **Figure 54** where also the separate contributions to μ_Δ from the different interaction processes are indicated for $\Delta = 200$ keV.

References

Anderson C (1932) The apparent existence of easily deflectable positives. *Science* 76(1967): 238.

Attix FH (1986) *Introduction to Radiological Physics and Radiation Dosimetry*. New York: Wiley.

Berger MJ and Hubbell JH (1990) *Program Manual. XCOM: Photon Cross Sections on a Personal Computer*. Gaithersburg, MD: National Institute of Standards and Technology.

Berger MJ, Hubbell JH, Seltzer SM, et al. (2005a) *XCOM: Photon Cross Section Database (version 1.3)*. Gaithersburg, MD: National Institute of Standards and Technology. Available:http://physics.nist.gov/xcom (2009, October).

Berger MJ, Coursey JS, Sucker DS, and Chang J (2005b) *ESTAR, PSTAR and ASTAR: Computer Programs for Calculating Stopping-Power Tables for Electrons, Protons and Helium Ions*. Gaithersburg, MD: National Institute of Standards and Technology. Available at: http://physics.nist.gov/Star.

Bethe H (1930) Zur Theorie des Durchgangs schneller Korpuskularstrahlen durch Materie. *Annalen der Physik* 397: 325.

Bethe H and Heitler W (1934) On the stopping of fast particles and on the creation of positive electrons. *Proceedings of the Royal Society of London A* 146: 83.

Bethge K, Kraft G, Kreisler P, and Walter G (2004) *Medical Applications of Nuclear Physics*. Heidelberg: Springer.

Bohr N (1913a) On the constitution of atoms and molecules. *Philosophical Magazine* 26: 1.

Bohr N (1913b) On the constitution of atoms and molecules/part II-systems containing only a single nucleus. *Philosophical Magazine* 26: 476.

Borsellino A (1953) Momentum transfer and angle of divergence of pairs produced by photons. *Physical Review* 89: 1023.

Brahme A (1975) Simple relations for the penetration of high energy electron beams in matter. SSI: 1975–011. Department of Radiation Physics, Karolinska Institutet, Stockholm, Sweden.

Brahme A (1978) Restricted energy absorption coefficients for use in dosimetry. *Radiation Research* 73: 420.

Brahme A and Svensson H (1976) Specification of electron beam quality from the central-axis depth absorbed-dose distribution. *Medical Physics* 3: 95.

Brahme A and Svensson H (1979) Radiation beam characteristics of a 22 MeV microtron. *Acta Radiologica Oncology* 18: 244.

Browne E and Firestone E (1986) *Table of Radioactive Isotopes*. New York: Wiley.

Brysk H and Zerby CD (1968) Photoelectric cross section in the keV range. *Physical Review* 171: 292.

Burlin TE (1966) A general theory of cavity ionization. *British Journal of Radiology* 39: 727.

Cerenkov PA (1934) Visible emission of clean liquids by action of γ-radiation. *Doklady Akademii Nauk SSSR* 2: 451.

Compton AH (1923) A quantum theory of the scattering of x-rays by light elements. *Physical Review* 21(5): 483.

Dirac PAM (1928) The quantum theory of the electron. *Proceedings of the Royal Society A: Mathematical Physical and Engineering Sciences* 117(778): 610.

Dirac PAM (1930) A theory of electrons and protons. *Proceedings of the Royal Society A: Mathematical Physical and Engineering Sciences* 126(801): 36.

Evans RD (1955) *The Atomic Nucleus*. Malabar, FL: Krieger.

Eyges L (1948) Multiple scattering with energy loss. *Physical Review* 74: 1534.

Fano U (1946) On the theory of the ionization yield of radiations in different substances. *Physical Review* 70: 44.

Fano U (1953) Gamma ray attenuation. *Nucleonics* 11, 8, 55.

Fermi E (1940) The ionization loss of energy in gases and in condensed materials. *Physical Review* 57: 485.

Geiger H and Marsden E (1909) On a diffuse reflection of the α-particles. *Proceedings of the Royal Society of London A* 82: 495.

Harder D (1965) Energiespektren schneller Elektronen in Vershiedenen Tiefen. In: Zuppinger A and Poretti G (eds.) *Symposium on High-Energy Electrons*, p. 260. Berlin: Springer.

Heitler W (1954) *The Quantum Theory of Radiation*. London and New York: Oxford University Press.

Higgins PD, Attix FH, Hubbell JH, Seltzer SM, Berger MJ, and Sibata CH (1991) *Mass Energy-Transfer and Mass Energy-Absorption Coefficients, Including In-Flight Positron Annihilation for Photon Energies 1 keV to 100 MeV*. NISTIR 4680. Gaithersburg, MD: National Institute of Standards and Technology.

Hollmark M, Gudowska I, Belkic Dž, Brahme A, and Sobolevsky H (2008) An analytical model for light ion pencil beam dose distributions: Multiple scattering of primary and secondary ions. *Physics in Medicine and Biology* 53: 3477.

Hubbell JH (1969) *Photon Cross Sections, Attenuation Coefficients and Energy Absorption Coefficients from 10 keV to 100 GeV*. Washington: National Bureau of Standards.

Hubbell JH, Veigele WJ, Briggs EA, Brown RT, Cromer D, and Howerton RJ (1975) Atomic form factors, incoherent scattering functions and photon scattering cross sections. *Journal of Physical and Chemical Reference Data* 4: 471.

Hubbell JH, Gimm HA, and Overbo I (1980) Pair, triplet and total atomic cross sections (and mass attenuation coefficients) for 1 MeV and 100 GeV photons in elements $Z = 1$ to 100. *Journal of Physical and Chemical Reference Data* 9: 1023.

Hultqvist M, Lazzeroni M, Botvina A, Gudowska I, Sobolevsky N, and Brahme A (2012) Evaluation of nuclear reaction cross-sections and fragment yields in carbon beams using the SHIELD-HIT Monte Carlo code. Comparison with experiments. *Physics in Medicine and Biology* 57: 4369.

ICRP (1973) Protection against Ionizing Radiation from External Sources: Supplement to ICRP Publication 15. ICRP Publication 21. Oxford. Pergamon Press.

ICRU (1984a) Radiation dosimetry: Electron beams with energies between 1 and 50 MeV. Report 35. Bethesda.

ICRU (1984b) Stopping powers for electrons and positrons. Report 37. Bethesda.

ICRU (1993) Stopping powers and ranges for protons and alpha particles. Report 49. Bethesda.

ICRU (2011) Fundamental quantities and units for ionizing radiation. International Commission on Radiological Units and Measurements Report 85. Bethesda.

Janek Straat S, Andreassen B, Jonsson C, et al. (2013) Clinical application of in vivo treatment delivery verification based on PET/CT imaging of positron activity induced at high energy photon therapy. *Physics in Medicine and Biology* 58: 5541.

Janek S, Svensson R, Jonsson C, and Brahme A (2006) Development of dose delivery verification by PET imaging of photonuclear reaction following high energy photon therapy. *Physics in Medicine and Biology* 51: 5769.

Jauch JM and Rorlich F (1955) *Theory of Photons and Electrons*. Berlin, Heidelberg: Springer, Verlag.

Kempe J and Brahme A (2008) Energy-range relation and mean energy variation in therapeutic particle beams. *Medical Physics* 35: 159.

Kempe J and Brahme A (2010) Analytical theory for the fluence, planar fluence, energy fluence, planar energy fluence and absorbed dose of primary particles and their fragments in broad therapeutic light ion beams. *Physica Medica* 26: 6, Epub Apr (2009).

Khan F (2003) *The Physics of Radiation Therapy*, 3rd ed. Baltimore, MD: Lippincott, Williams and Wilkins.

Klein O and Nishina Y (1929) Über die Streuung von Strahlung durch freie Elektronen nach der neuen relativistischen Quantendynamik von Dirac. *Zeitschrift für Physik* 52: 853.

Lazzeroni M and Brahme A (2011) Production of clinically useful positron emitter beams during carbon ion deceleration. *Physics in Medicine and Biology* 56: 1585.

McKinley WA Jr. and Feshbach H (1948) The coulomb scattering of relativistic electrons by nuclei. *Physical Review* 74: 1759.

Mott NF (1929) The scattering of fast electrons by atomic nuclei. *Proceedings of the Royal Society of London A* 124: 425.

Mott NF (1932) The full polarisation of electrons by double scattering. *Proceedings of the Royal Society of London A* 135: 429.

Motz JW and Missoni G (1961) Compton scattering by K-shell electrons. *Physical Review* 124: 1458.

Motz J, Olsen HA, and Koch HW (1969) Pair production by photons. *Reviews of Modern Physics* 41: 581.

Nikjoo H, Uehara S, and Emfietzogiou D (2012) *Interaction of Radiation with Matter*. London: Taylor and Francis.

Nilsson B and Brahme A (1981) Contamination of high-energy photon beams by scattered photons. *Strahlentherapie* 157: 181.

Nilsson B and Brahme A (1983) Relation between kerma and absorbed dose in photon beams. *Acta Radiologica. Oncology* 22: 77.

Nordell B and Brahme A (1984) Angular distribution and yield from bremsstrahlung targets (for radiation therapy). *Physics in Medicine and Biology* 29: 797.

Øverbø I, Mork KJ, and Olsen HA (1968) Exact calculation of pair production. *Physical Review* 175: 1978.

Perrin F (1933) Possibilit de materialisation par interaction d'un photon et d'un electron. *Comptes Rendus* 197: 1100.

Podgorsak EB (2009) *Radiation Physics for Medical Physicists*. Berlin: Springer.

Racah G (1936) Sula nascita di coppie per urti di particielle elettrizitate. *Nuovo Cimento* 13: 66.

Roy RR and Reed RD (1968) *Interactions of Photons and Leptons with Matter*. New York: Academic Press.

Rutherford E (1911) The scattering of α and β particles by matter and the structure of the atom. *Philosophical Magazine Series 6* 21: 669.

Svensson R and Brahme A (1996) Effective source size, yield and beam profile from multilayered bremsstrahlung targets. *Physics in Medicine and Biology* 41: 1353.

Thomson JJ (1933) *Conduction of Electricity through Gases*II: London and New York: Cambridge University Press.

Trubey DK, Berger MJ, and Hubbell JH (1989) *Photon Cross Sections for ENDF/B-VI*. CONF-890408-4Gaithersburg, MD: NIST.

Zhou S-A and Brahme A (2008) Development of phase-contrast X-ray imaging techniques and potential medical applications. *Physica Medica* 24: 129.